

Lattice QCD at non-zero temperature

P. Petreczky

Physics Department, Brookhaven National Laboratory, Upton, NY 11973, USA

Abstract. I review our current understanding of the properties of strongly interacting matter at high temperatures, based upon numerical calculations in lattice QCD. I discuss the chiral and deconfining aspects of the QCD transition, the equation of state, fluctuations of conserved charges, color screening, meson correlation functions, and the determination of some transport coefficients.

1. Introduction

It is expected that strongly interacting matter shows qualitatively new behavior at temperatures and/or densities which are comparable or larger than the typical hadronic scale. It has been argued by Hagedorn that production of hadronic resonances may lead to a limiting temperature above which hadronic matter can no longer exist [1]. This limiting temperature was re-interpreted by Cabibbo and Parisi as the transition temperature to a new state of matter that consist of quarks [2]. Indeed, based of asymptotic freedom one would expect that relevant degrees of freedom at very high temperatures and/or densities are quarks and gluons which are no longer subject to confinement [3], i.e. deconfined. Since the quarks and gluons interact weakly at high temperatures the deconfined matter is analogous to the plasmas and is also called the quark gluon plasma (QGP) [4]. In particular, it is characterized by color screening that is similar to the well-know Debye screening [5].

The existence of such deconfining transition was first shown using strong coupling expansion in lattice QCD [6, 7], followed by numerical Monte-Carlo studies of the lattice $SU(2)$ gauge theory which confirmed it [8, 9, 10]. The deconfinement of gluons was seen as onset of color screening [8, 9] and rapid increase in the energy density that indicate liberation of many new degrees of freedom [10]. The onset of color screening and rapid increase in number of degrees of freedom remain the key signatures of deconfinement even today.

Since these pioneering studies QCD at finite temperature became quite a large sub-field of lattice QCD. One of the obvious reasons for this is that the transition from hadronic to partonic matter cannot be described in perturbation theory. But even at high temperatures the physics is non-perturbative beyond the length scales $1/(g^2 T)$ (g^2 being the gauge coupling) [11]. Therefore lattice QCD remains the only ab-initio tool for theoretical understanding of the properties of strongly interacting matter under

extreme condition which is important for the physics of the early universe [12, 13, 14] and heavy ion collisions [15].

Symmetries play an important role in understanding the transition to QGP. For zero quark masses the QCD Lagrangian has an approximate chiral symmetry $SU_A(3)$ as well as the axial symmetry $U_A(1)$. The later is broken by quantum effects, while the former is spontaneously broken by the QCD vacuum [16]. At high temperatures the chiral symmetry is expected to be restored [17]. Therefore there should be a chiral transition in QCD. The nature of the chiral transition was first discussed in Ref. [18], where it was argued that for three light quark flavors the transition should be first order, while for two flavors it could be second order belonging to the $O(4)$ universality class. Furthermore, the axial symmetry is also effectively restored at high temperatures as the breaking of the axial symmetry is controlled by instanton density [18] that vanishes at infinite temperature [17]. If the breaking of axial symmetry at the chiral transition temperature is reduced the chiral transition in the two flavor theory could be first order [18]. I will comment on this issue in section 5.

In the opposite limit of infinitely heavy quark masses the QCD partition function has $Z(3)$ symmetry [9]. This symmetry is broken at high temperatures due to color screening. In this case we have a deconfining transition which is first order. The $Z(3)$ symmetry is a good symmetry for sufficiently large quark mass. For intermediate quark masses the transition is a crossover. The regions of the first order transitions are separated from the crossover region by lines of second order transition that belong the $Z(2)$ universality class. The region of the first order deconfinement transition was mapped out in Refs. [19, 20, 21]. The endpoints of this first order region correspond to a quark masses of the order of the charm quark mass, $m_q \sim 1.4\text{GeV}$ [19, 20].

The boundary of the first order chiral transition was studied using effective models, see Refs. [22, 23] for recent works (also references therein). It was found that for three degenerate quark flavors the endpoint of the region where the transition is first order corresponds to a pseudo-scalar meson mass of $(110 \pm 40)\text{MeV}$. There is no direct evidence for the first order chiral transition for three very light quark flavors so far in lattice QCD. This maybe due to lattice artifacts. The existing calculations that use staggered fermion formulation give only an upper bound for the pseudo-scalar meson mass smaller than 70MeV [24, 25, 26], which is not inconsistent with effective model analysis mentioned above. The end-point of the first order transition, or in more general case the line that separates the first order transition from the crossover region belongs to the $Z(2)$ universality class. This also means that for some value of the strange quark mass, m_s^{TCP} we have a tricritical point that connects $Z(2)$ and $O(4)$ lines as well as the first order region. Calculations in linear sigma model suggest that m_s^{TCP} corresponds to the kaon mass of about $(1700 - 1850)\text{MeV}$ [23]. On the other hand, as we will see, lattice QCD calculations indicate a much smaller value of m_s^{TCP} . The above picture of the finite temperature QCD transition is summarized in Fig. 1 (also known as the Columbia plot).

For the physical quark masses the transition is likely to be an analytic crossover [27]

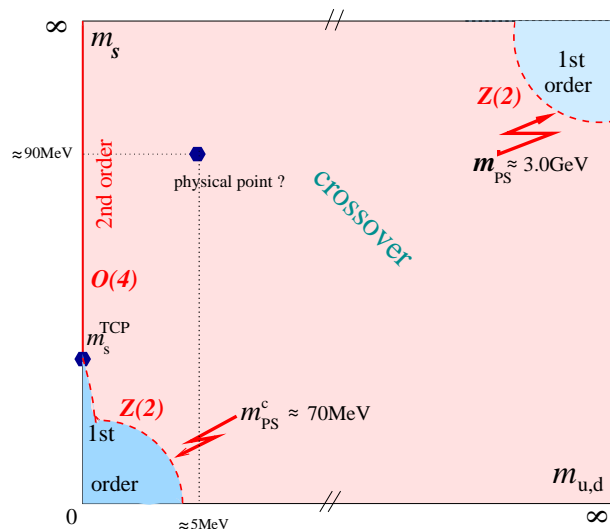


Figure 1. The QCD transition as function of the quark masses.

(for earlier works see Refs. [28, 29]). Therefore, the discussion of the deconfinement and the chiral aspects of the QCD transition at finite temperature and the determination of the corresponding temperature requires a special care. In fact, it is only the chiral aspects of the transition that allow a determination of the corresponding transition temperature. In sections 3 and 4 I discuss the deconfinement aspects of the QCD transition in terms of chromo-electric screening and fluctuations of conserved charges. The chiral aspects of the QCD transition and the determination of the corresponding transition temperature are then discussed in section 5. Equation of state is one of the most important characteristic of hot strongly interacting medium. It will be discussed in section 5. Further insight into the properties of medium can be gained by studying meson correlation functions and spectral functions. They are also important for heavy ion phenomenology. Therefore section 7 is dedicated to the discussion of meson correlation functions and spectral functions. In the next section I will review some basic information on lattice QCD calculations which is relevant for the present discussions.

2. Basics of lattice QCD

To study QCD non-perturbatively we use lattice gauge theory [30]. In this formalism a field theory is defined in a gauge-invariant way on a discrete space-time domain. This serves at least two purposes: a) to provide an ultra-violet cut-off for the theory, restricting highest momentum to π/a (a being the lattice spacing), and b) to evaluate the path integrals in the Euclidean formulation stochastically using importance sampling.

On the lattice the fundamental degrees of freedom of a theory with local $SU(3)$ gauge symmetry are fermion fields ψ_x that reside on the sites of the lattice and carry flavor, color and Dirac indices, which we suppress through the most of this paper, and bosonic, gauge degrees of freedom that in the form of $SU(3)$ matrices $U_{x,\mu}$ reside on links. Sites on a four-dimensional lattice are labeled with $x \equiv (\tau, \vec{x})$. The link variables

are related to the usual gauge fields: $U_{x,\mu} = \exp(igaA_\mu(x))$, where a is the lattice spacing and g is the gauge coupling.

The theory is defined by the partition function

$$Z = \int DU D\bar{\psi} D\psi \exp(-S) \quad (1)$$

where the action

$$S = S_g + S_f \quad (2)$$

contains gauge, S_g and fermionic, S_f parts. The latter part is bi-linear in fields and has the form

$$S_f = \sum_q \bar{\psi}_q D_q \psi_q \quad (3)$$

where $D_q = D + m_q$ is the fermion matrix and the sum goes over the quark flavors. In the simplest formulation the lattice gauge action can be written as

$$S_g = \beta \sum_{x,\mu < \nu} \left(1 - \frac{1}{3} \text{Re Tr } U_{x,\mu} U_{x+\hat{\mu},\nu} U_{x+\hat{\nu},\mu}^\dagger U_{x,\nu}^\dagger \right), \quad (4)$$

$\beta = 6/g^2$ with g^2 being the bare gauge coupling. This is the Wilson gauge action [30]. It is easy to see that expanding the link variables in a the above expression gives the well known Yang-Mills action $\sum_x a^4 1/4 (F_{\mu\nu}^a)^2$ up to corrections that are suppressed as a^2 . Thus calculations with Wilson gauge action have discretization errors of order a^2 . These discretization errors can be removed by the Symanzik improvement program that relies on higher order difference scheme, i.e. considering combination of link variables that extend beyond the elementary square [31].

The expectation value of an operator \hat{O} is then given by

$$\langle \hat{O} \rangle = \frac{1}{Z} \int DU D\bar{\psi} D\psi \hat{O} \exp(-S). \quad (5)$$

Integration over the fermion fields (which are Grassmann variables) can be carried out explicitly:

$$Z = \int DU (\det D_q[U])^{n_f} \exp(-S_g) \equiv \int DU \exp(-S_{eff}), \quad (6)$$

where $S_{eff} = S_g - n_f \ln \det D_q[U]$ is the effective action. The fermion determinant $\det D_q[U]$ describes the vacuum polarization effects due to the dynamical quarks and makes the effective action non-local in gauge variables. For this reason simulations with dynamical quarks are very resource demanding and the quenched approximation is often employed, where $\det D_q[U]$ is set to 1. This approximation will be relevant for the discussion of the meson spectral functions.

The most commonly used fermion formulations include : the Wilson fermion formulation, staggered fermion formulation [32] and the domain wall fermion (DWF) formulation [33, 34, 35]. The Wilson formulation breaks the chiral symmetry of the QCD Lagrangian. As the result quark masses acquire an additive renormalization which makes the calculations quite complicated and numerically expensive. The domain wall fermions preserve all the symmetry of the QCD Lagrangian at a price on introducing the extra

fifth dimension. Therefore the computational costs associated with DWF formulation are proportional to the extent of the fifth dimension and are typically 30 to 100 times larger than the ones with Wilson fermions. The staggered formulation describes four fermion flavors (also called tastes) in the continuum limit. The full $U_L(4) \times U_R(4)$ symmetry of the four flavor theory is reduced to $U_S(1) \times U_B(1)$, where $U_S(1)$ is the subgroup of the $SU_A(4)$ symmetry. Thus the staggered formulation preserves a part of the chiral symmetry. This makes finite temperature calculations with staggered fermions attractive for two reasons. First, due to the remnant chiral symmetry there is no additive renormalization of the quark mass. This makes staggered fermions computationally inexpensive. Second, the remnant chiral symmetry makes it easy to study the chiral aspects of the finite temperature QCD transitions. To study arbitrary number of flavors with the staggered fermion formulation the rooting trick is used. This amounts to replacing n_f in Eq. (6) with $n_f/4$. The validity of this procedure was studied in details in recent years [36, 37, 38, 39, 40, 41, 42] though some open issues remain (see e.g. Ref. [38, 43]).

The standard staggered fermion formulations has discretization errors of order a^2 . They come either from the lattice effects in the fermion dispersion relation and formally start at order $g^0 a^2$, and from the breaking of taste symmetry, which starts at order $g^2 a^2$. The former lead to large cutoff effects in the thermodynamic quantities at high temperatures. The later lead to the distortion of the hadron spectrum at non-zero lattice spacing. In particular, out of 16 pseudo-scalar meson masses only one vanishes in the zero quark mass limit. The remaining 15 pseudo-scalar meson have masses proportional to a (the squared mass of these mesons goes like $g^2 a^2$ for sufficiently small lattice spacings) and thus vanish only in the continuum limit. These discretization errors can be eliminated by Symanzik improvement program. Using 3-link terms in the lattice Dirac operator one can eliminate tree level a^2 errors and largely reduce cutoff effects in thermodynamics quantities [44]. Such improvement of the staggered fermion formulation is mandatory to control discretization effects at high temperature [44]. To reduce errors due to taste symmetry breaking so-called fat links are used. These are combinations of the usual link $U_{x,\mu}$ and products of links along different paths. One of the possibilities is to construct fat links by using APE smearing [45]: a link variable $U_{x,\mu}$ is replaced by a weighted average of itself and a sum of the 3-link paths connecting the same sites as $U_{x,\mu}$:

$$U_{x,\mu} \rightarrow U'_{x,\mu} = (1 - 6c)U_{x,\mu} + c \sum_{\nu \neq \mu} U_{x,\mu} U_{x+\hat{\nu},\mu} U_{x+\hat{\mu},\nu}^\dagger. \quad (7)$$

Here c is a weight factor, $0 < c < 1$. More complicated paths can be used as well. In particular, using combination of different paths up to length seven it is possible to eliminate taste breaking effects up to order $g^2 a^2$ [46]. The fat links described above are not elements of the gauge group $SU(3)$. While this is not a problem in principle, it turns out that projecting the fat links to elements of $SU(3)$ or $U(3)$ gauge group further reduces the breaking of taste symmetry [47, 48, 49]. The staggered fermion actions that used in large numerical calculations take certain combination of fat links

and improvement of the quark dispersion relation and go under acronym *p4*, *asqtad* and *HISQ/tree*. In *HISQ/tree* action the fat links are projected to $U(3)$ [50]. The *stout* action used by Budapest-Wuppertal collaboration only includes fat links [51, 52, 27, 53].

To evaluate the path integral (5) stochastically, an ensemble of N_U gauge configurations, weighted with $\exp(-S_{eff})$, is generated using Monte Carlo methods. The state of the art Monte-Carlo algorithm that can handle arbitrary number of quark flavors and most often used in QCD thermodynamics goes under the name of the rational hybrid Monte-Carlo (RHMC) algorithm [54]. The expectation value of the operator is then approximated by the ensemble average:

$$\langle \hat{O} \rangle \simeq \frac{1}{N_U} \sum_{i=1}^{N_U} O_i(U), \quad (8)$$

where $O_i(U)$ is the value of the operator \hat{O} , calculated on i -th configuration. This method works as long as S_{eff} is real. When quark chemical potentials are included, e.g. as in calculations at non-zero net baryon density, S_f and S_{eff} become complex and Monte-Carlo methods do not work. This is the well known sign problem.

All the quantities calculated in lattice simulations are dimensionless, i.e. are calculated in units of the lattice spacing a . The lattice spacing is varied by varying the lattice gauge coupling $\beta \sim 1/g^2$. To set the scale in lattice simulations we need to calculate a given quantity and assume that it has the known physical value. Different choices are possible and the lattice spacing determined by different quantities should be the same up to discretization errors that vanish when the continuum limit is taken. Common choices used in the literature are the scale parameters r_0 and r_1 determined by the static quark anti-quark potential $V(r)$:

$$r^2 \frac{dV}{dr} \Big|_{r=r_0} = 1.65, \quad r^2 \frac{dV}{dr} \Big|_{r=r_1} = 1.00 \quad (9)$$

Since the static quark anti-quark potential cannot be measured experimentally the value of the parameters r_0 and r_1 in physical units in the continuum should be determined using some other experimentally measured quantity. The most precise determination of r_1 comes from using the pion decay constant f_π as an input, which gives $r_1 = 0.3106(20)\text{fm}$ [55]. Furthermore, studying the shape of the static potential from the above value of r_1 one can obtain the value of $r_0 = 0.468(4)\text{fm}$ [56]. Alternatively one can use f_K to set the lattice spacing. While this procedure is more straightforward, for the staggered fermion formulation it is also more problematic as one expects that due to taste symmetry breaking f_K has larger discretization errors than the static potential.

The above discussion referred to the zero temperature case. To consider the case of non-zero temperature, T the Euclidean time extent has to be $1/T$ and periodic and anti-periodic boundary condition have to be imposed on the boson and fermion fields [57]. Thus the temperature is related to the lattice spacing and the temporal extent of the lattice, $T = 1/(N_\tau a)$. Taking the continuum limit at fixed temperature implies $N_\tau \rightarrow \infty$ while keeping the aspect ratio N_σ/N_τ fixed, where N_σ is the spatial extent of the lattice.

3. Deconfinement : color screening

3.1. Color electric screening and order parameter for deconfinement

As discussed in the introduction the deconfining transition in $SU(N)$ gauge theories is a true phase transition related to $Z(N)$ symmetry \ddagger . The order parameters of this phase transition are the expectation value of the Polyakov loop and the Polyakov loop correlator

$$L(T) = \langle \frac{1}{N} \text{Tr} W(\vec{x}) \rangle, \quad W(\vec{x}) = \prod_{\tau=0}^{N_\tau-1} U_0(\tau, \vec{x}), \quad (10)$$

$$C_{PL}(r, T) = \frac{1}{N^2} \langle \text{Tr} W(r) \text{Tr} W(0) \rangle. \quad (11)$$

The Polyakov loop transforms non-trivially under $Z(N)$ transformation and the expectation value of the Polyakov loop is zero in the confined phase and non-zero above the transition temperature. The correlation function of the Polyakov loop is related to the free energy of a static quark anti-quark pair [9]. The qualitative change in the behavior of the Polyakov loop and its correlator above the phase transition temperature is related to color screening. As it was pointed out already in Ref. [9] the Polyakov loop and the Polyakov loop correlator require renormalization to be interpreted as the free energy of an isolated static quark or the free energy of a static quark anti-quark ($Q\bar{Q}$) pair. More precisely, they are related to the free energy difference of a system with static $Q\bar{Q}$ pair at some temperature and the system without $Q\bar{Q}$ pair at the same temperature. Since in the zero temperature limit the free energy of a static quark anti-quark pair should coincide with the static potential the Polyakov loop renormalization is determined by the normalization constant of the static potential, namely

$$L_{ren}(T) = \exp(-c/(2T))L(T) = \exp(-F_\infty(T)/(2T)) \quad (12)$$

$$C_{PL}(r, T) = \exp(-F(r, T)/T + c/T), \quad F_\infty(T) = \lim_{r \rightarrow \infty} F(r, T), \quad (13)$$

where c is an additive normalization that ensures that the static potential has a certain value at a given distance. In the above expressions we made explicit that the free energy of an isolated static quark anti-quark pair is half the free energy of $Q\bar{Q}$ pair at infinite separation. In the confined phase the free energy of a static quark anti-quark pair is proportional to $\sigma(T)r$ at large distances r , as expected. The effective temperature dependent string tension $\sigma(T)$ is non-zero below the phase transition temperature [61, 62]. Consequently the free energy of an isolated static quark is infinity and $L_{ren}(T) = 0$. In the deconfined phase $F_\infty(T)$ is finite due to color screening. In particular at high temperatures $F_\infty = -4\alpha_s m_D/3$ at leading order, where $m_D = gT$ is the leading order Debye mass. Here and in what follows we consider only the case $N = 3$. The next-to-leading order correction for F_∞ has been calculated in Refs. [63, 64]

\ddagger The deconfinement transition for other gauge groups have been discussed in Refs.[58, 59, 60].

and was found to be small. For the free energy of a static $Q\bar{Q}$ pair at distance r we have [65]

$$F(r, T) = -\frac{1}{9} \frac{\alpha_s^2}{r^2} \exp(-2m_D r). \quad (14)$$

This result is in contrast to the free energy of static charges in QED which is $-\alpha \exp(-m_D r)/r$, and is the consequence of non-Abelian nature of interactions. A static quark anti-quark pair could be either in a singlet or in an octet state, and thus (in a fixed gauge) one can define the so-called color singlet and octet free energy [65, 66]

$$\exp(-F_1(r, T)/T + c/T) = \frac{1}{3} \langle \text{Tr}[L^\dagger(x)L(y)] \rangle, \quad (15)$$

$$\begin{aligned} \exp(-F_8(r, T)/T + c/T) &= \frac{1}{8} \langle \text{Tr} L^\dagger(x) \text{Tr} L(y) \rangle \\ &\quad - \frac{1}{24} \langle \text{Tr} [L^\dagger(x)L(y)] \rangle. \end{aligned} \quad (16)$$

Then the Polyakov loop correlator can be written as the thermal average over the singlet and the octet contributions [9, 65, 66]

$$C_{PL}(r, T) = \frac{1}{9} \exp(-F_1(r, T)/T + c/T) + \frac{8}{9} \exp(-F_8(r, T)/T + c/T). \quad (17)$$

The singlet and octet free energies can be calculated at high temperature in leading order HTL approximation [71], resulting in

$$F_1(r, T) = -\frac{4}{3} \frac{\alpha_s}{r} \exp(-m_D r) - \frac{4\alpha_s m_D}{3}, \quad (18)$$

$$F_8(r, T) = \frac{1}{6} \frac{\alpha_s}{r} \exp(-m_D r) - \frac{4\alpha_s m_D}{3}. \quad (19)$$

The singlet and octet free energies are gauge independent at this order. Inserting the above expressions into Eq. (17) and expanding in α_s one can see that the leading order contributions from the singlet and octet channels cancel each other and one recovers the leading order result for $F(r, T)$ in Eq. (14). It was not clear how to generalize the decomposition of the free energy into the singlet and octet contributions beyond leading order. Recently using the effective theory approach, namely the potential non-relativistic QCD (pNRQCD) at finite temperature [72, 73] it was shown that this decomposition indeed holds at short distances [64]. As we will see below the singlet free energy turns out to be useful when studying screening numerically in the lattice calculations.

The QCD partition function does not have the $Z(3)$ symmetry. This symmetry is broken by the quark contribution. In physical terms this means that a static quark anti-quark pair can be screened already in the vacuum by light dynamical quarks. The free energy does not rise linearly with distance but saturates at some distance, i.e.

§ The terms color singlet free energy and octet free energy are misleading as only $F(r, T)$ has the meaning of the free energy of static quark anti-quark pair. Furthermore, at low temperatures both F_1 and F_8 are determined by color singlet asymptotic states [67]. The color screening of static quark quark interaction was discussed in Ref. [68], while color screening of charges in higher representations was studied in Refs. [69, 70].

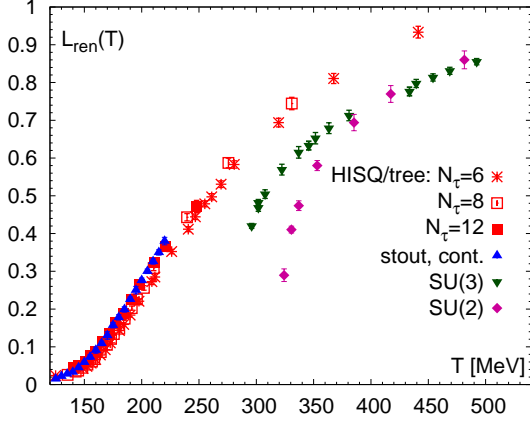


Figure 2. The Polyakov loop as function of the temperature in 2+1 flavor QCD [74, 56] and in pure gauge theory [62, 75].

we see string breaking. For light dynamical quarks the corresponding free energy F_∞ is twice the binding energy of static-light meson and thus is proportional to Λ_{QCD} . Therefore, the Polyakov loop is expected to be $\mathcal{O}(1)$ in the transition region. At very high temperatures, however, the screening in the QCD and purely gluonic plasma is expected to be similar. The above discussion of the free energy of static quark anti-quark pair still holds and the only difference is in the value of the Debye mass, which now becomes $m_D = gT\sqrt{1 + N_f/6}$. Here N_f being the number of light quark flavors, i.e. $N_f = 3$.

In Fig. 2 I show the recent lattice results for the renormalized Polyakov loop in 2+1 flavor QCD with physical quark masses [74] compared to the results in pure gluodynamics [62, 75]. The temperature scale in pure gauge theory was set using the value $\sqrt{\sigma} = 465.2\text{MeV}$ for the zero temperature string tension. We see a relative smooth increase in the Polyakov loop in 2+1 flavor QCD starting at temperatures of about 160 MeV. Earlier results for the renormalized Polyakov loop in 2 and 3 flavor QCD with significantly heavier quark masses have been reported in Refs. [76, 77]. The behavior of the Polyakov loop in pure glue theory and full QCD is quite different in the transition region, while at high temperatures it is qualitatively similar.

The free energy of a static $Q\bar{Q}$ pair as well as the singlet free energy was calculated using $p4$ action on $16^3 \times 4$ and $24^3 \times 6$ lattices for almost physical light quark masses, namely $m_l = m_s/10$ [78, 79]. There are also calculations with Wilson fermion formulation with much heavier quark masses [80] as well as preliminary results for the *stout* action [81]. Qualitatively these results are similar to the ones obtained with $p4$ action. A very detailed calculation of the free energy of $Q\bar{Q}$ pair in pure glue theory was presented in Refs. [61, 62, 82], while the singlet free energy in Coulomb gauge was studied in Refs. [75, 83].

In Fig. 3 I show the numerical results for the free energy and the singlet free energy obtained with $p4$ action on $16^3 \times 4$ lattice. At low temperatures the qualitative behavior

of the free energy and singlet free energy is similar. The singlet free energy agrees with the zero temperature potential shown in the figure as the black line, while the free energy differs from it by the trivial color factor $T \ln 9$. At high temperatures the free energy and the singlet free energy show very different behavior, in particular the temperature dependence is much stronger in $F(r, T)$. The singlet free energy agrees with the zero temperature potential at short distances, while this is not the case for the free energy even when the factor $T \ln 9$ is taken into account. This behavior of the $Q\bar{Q}$ free energy at high temperatures is consistent with the partial cancellation of the color singlet and color octet contributions as described above. Similar difference between the free energy and singlet free energy have been observed in the pure glue theory [61, 75, 82].

Color screening means that $r(F_1(r, T) - F_\infty(T))$ as well as $r(F(r, T) - F_\infty(T))$ should decay exponentially at large distances. Therefore in Fig. 4 I show these combinations. At distance $rT > 0.8$ we indeed see the expected exponential falloff. Fitting the lattice data for $r(F_1(r, T) - F_\infty(T))$ to an exponential one can determine the Debye mass non-perturbatively. This was done for pure glue theory and 2+1 flavor QCD. It turns out that the temperature dependence of the Debye mass is well described by the leading order result but its value is about factor 1.4 larger both in pure glue theory and 2+1 flavor QCD [79] ||. This means that the dependence of the Debye mass on quark flavors is well described by perturbation theory. The Debye mass is non-perturbative beyond leading order [84, 85]. The non-perturbative enhancement of the Debye mass over the leading order result is expected based on the gap equation calculation of the Debye mass [86].

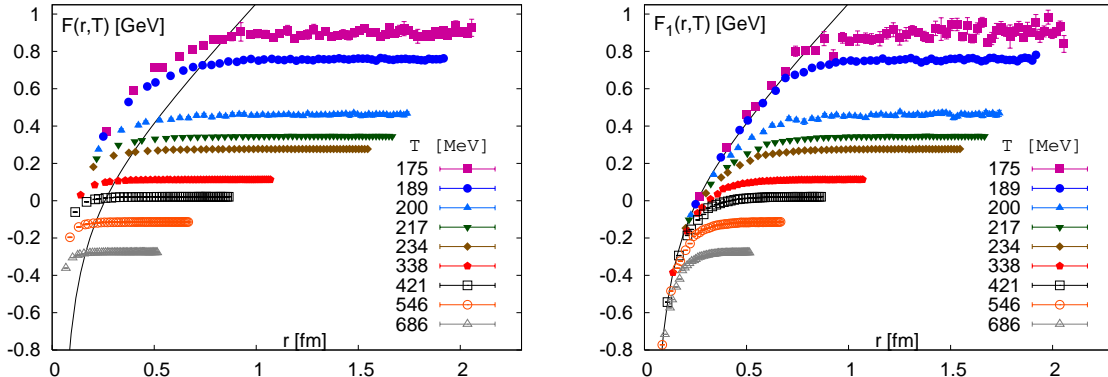


Figure 3. The free energy (left) and the singlet free energy (right) of a static $Q\bar{Q}$ pair calculated in 2+1 flavor QCD on $16^3 \times 4$ lattices at different temperatures [78]. The solid black line is the parametrization of the zero temperature potential calculated in Ref. [87].

The qualitative features of the singlet free energy discussed above are not specific to the Coulomb gauge. In fact, the singlet free energy defined in terms of Wilson loops show very similar behavior to the one calculated in the Coulomb gauge [88]. Furthermore,

|| The Debye mass obtained in the calculations with Wilson fermions is somewhat larger [80]. More calculations are needed to resolve this discrepancy.

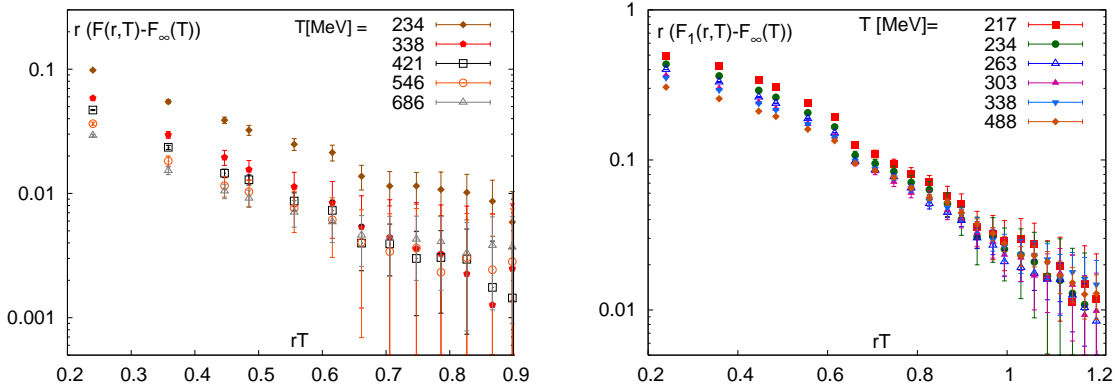


Figure 4. The combination $r(F(r,T) - F_\infty(T))$ (left) and $r(F_1(r,T) - F_\infty(T))$ (right) for different temperatures as function of rT [78].

the Debye mass can also be defined from the long distance behavior of the electric gluon propagator [89, 90, 91, 92, 93, 94]. Calculations in $SU(2)$ and $SU(3)$ gauge theories show no gauge dependence of the extracted Debye mass within statistical errors [92, 93]. The extracted screening masses are in agreement with the ones obtained from the singlet free energy

3.2. Color magnetic screening and dimensional reduction

Contrary to ordinary plasmas that have no magnetic screening the static chromo-magnetic fields are screened in QGP. This is due to the fact that unlike photons gluons interact with each other (the stress tensor is non-linear in QCD). Magnetic screening is non-perturbative, i.e. it does not appear at any finite order of perturbation theory and is needed to cure the infrared divergences of the pressure rendering it finite but also non-perturbative at order g^6 [11]. In analogy with electric screening magnetic screening can be studied using gauge fixed magnetic gluon propagators. However, the large distance behavior of the magnetic propagators is more complex and much more susceptible to finite volume effects. In Landau type gauges as well as in Coulomb gauge the magnetic propagator shows oscillating behavior instead of decaying exponentially [95]. Thus no magnetic mass can be defined. However, one can define a common exponentially falling envelope for different gauges that then gives a screening mass of about $0.5g^2T$ [95]. A magnetic mass of similar size was found in analytic approach of Refs. [96, 97, 98]. Thus the corresponding effective magnetic screening length is larger than the electric screening length as one would expect for weakly coupled QGP ¶.

Spatial Wilson loops can also be used to define a length scale associated with static magnetic fields. They obey area law at any temperature governed by spatial string tension $\sigma_s(T)$. The numerical results for the spatial string tension calculated in 2+1 flavor QCD with $p4$ action and $m_l = m_s/10$ are shown in Fig. 5. At low

¶ Speculations on existence of a magnetic screening length of similar size have been presented in Ref. [99]

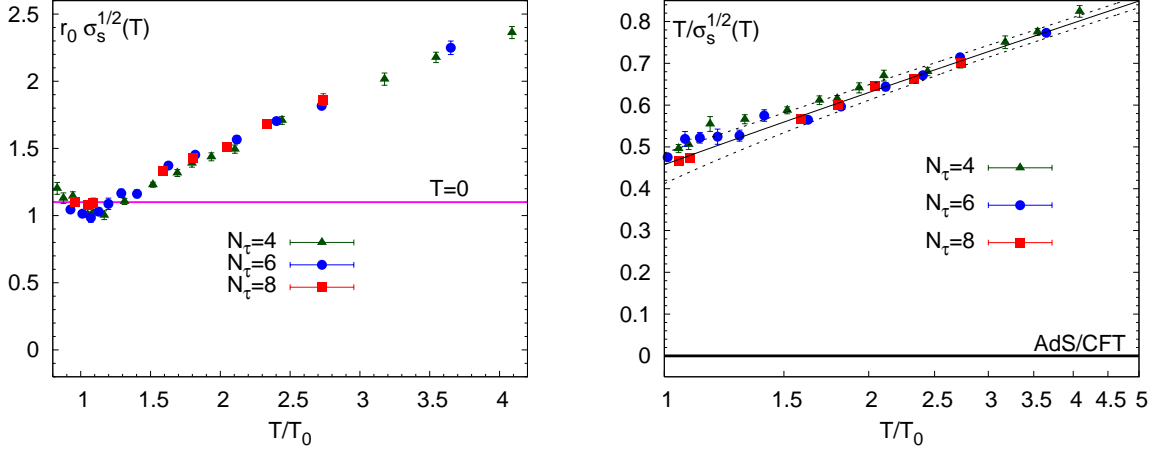


Figure 5. (Left) The string tension in units of r_0 as function of the temperature calculated on $N_\tau = 4, 6$ and 8 lattices. For better visualization we scale the temperature axis by $T_0 = 200\text{MeV}$. (Right) $T/\sqrt{\sigma_s(T)}$ calculated on $N_\tau = 4, 6$ and 8 lattices compared with the prediction of dimensional reduction indicated by the line. The uncertainty in the prediction of the dimensionally reduced theory is shown by dashed lines.

temperatures $\sigma_s(T)$ coincides with the zero temperature string tension, while at high temperatures $\sqrt{\sigma_s(T)} \sim T$. This behavior can be understood in terms of dimensionally reduced effective theory. At high temperatures there is a separation of different scales $2\pi T \gg m_D \gg g^2 T$. If we integrate out the modes associated with the scale $2\pi T$ the thermodynamics and the screening lengths can be described in terms of an effective field theory, which at the lowest order is the 3 dimensional adjoint Higgs model in the confined phase [100, 101, 102]

$$S_3^E = \int d^3x \frac{1}{g_3^2} \text{Tr} F_{ij}(\mathbf{x}) F_{ij}(\mathbf{x}) + \text{Tr} [D_i, A_0(\mathbf{x})]^2 + m_D^2 \text{Tr} A_0(\mathbf{x})^2 + \lambda_A (\text{Tr} A_0(\mathbf{x})^2)^2. \quad (20)$$

The static electric fields become adjoint scalars in the three dimensional effective theory. The couplings of the effective theory can be calculated in perturbation theory at any order [101, 102]. The spatial string tension should be identified with the string tension of this effective three dimensional theory σ_3 . The gauge coupling constant in three dimensions g_3^2 has the dimension of the mass, and at the lowest order (tree level) $g_3^2 = g^2 T$. On dimensional grounds $\sigma_3 = c g_3^2$ with c being a constant. This explains the linear rise of the string tension at high temperatures. The coefficient c was calculated in the three dimensional adjoint Higgs model [103, 104]. The three dimensional gauge g_3 coupling was calculated to 2-loop [105]. Combining this with the known value of c we get the weak coupling prediction for the spatial string tension which is compared with the lattice data in Fig. 5. Quite surprisingly, the weak coupling result for the spatial string tension works well down temperatures of 200MeV , where the effective field theory is not supposed to work. Note that in the conformal strongly coupled gauge theory $T/\sqrt{\sigma_s(T)} \sim 1/\lambda^{1/4}$ (see e.g. Ref. [106] and references therein). Thus the

ratio $T/\sqrt{\sigma_s(T)}$ is temperature independent and vanishes in the limit of infinite t'Hooft coupling, $\lambda \rightarrow \infty$. This is in sharp contrast with lattice calculations. To deal with this problem one can modify the AdS metric to break the conformal invariance and get a QCD-like theory. This approach is known as AdS/QCD. Attempts to model the temperature dependence of the spatial string tension using AdS/QCD were discussed in Ref. [107, 108, 109].

3.3. The spectrum of gauge invariant screening masses

There are several screening masses that can be studied in the framework of the 3 dimensional effective theory [110, 111, 112, 103, 104] as well as in the original four dimensional theory [113, 114, 115, 62]. Comparison of the screening masses calculated in these two theories can provide information on the validity of the dimensionally reduced effective theory. The screening masses can be classified according to J^{PR} quantum numbers. Here R is the analog of C-parity. It is related to the symmetry with respect to the following transformation of the static electric field, $A_0 \rightarrow -A_0$. All the operators transform trivially under charge conjugation in the adjoint Higgs model [103]. In the 0^{++} channel there are two distinct screening masses: screening mass $m(A_0^2)$ corresponding to the “electric” correlator of $\text{Tr}A_0^2$, and the screening mass m_G corresponding to the “magnetic” correlator $\text{Tr}F_{ij}^2$. These correlators can mix but this mixing is suppressed for weak coupling. The lightest screening mass m_E in the 0^{--} channel was proposed as the non-perturbative definition of the Debye mass [116] since the negative R parity prevents mixing with the magnetic sector. For asymptotically small couplings we expect $m_G < m_E < m(A_0^2)$ and the large distance behavior of the Polyakov loop correlators is actually governed by the “magnetic” screening mass m_G [116, 117]. For the interesting temperature range, however, $m(A_0^2)$ turns out to be the smallest and m_G turns out to be the largest of the above screening masses [103, 104]. Furthermore, there is almost no mixing between the “electric” and “magnetic” correlators in the 0^{++} channel [103, 104]. Thus the long distance behavior of the Polyakov loop is determined by the screening mass corresponding to $\text{Tr}A_0^2$ correlator (see also discussion in Ref. [117]). In Fig. 6 I show the screening masses extracted from the Polyakov loop correlators in $SU(2)$ and $SU(3)$ gauge theories and compared to the corresponding screening masses calculated in the effective three dimensional theory. There is fairly good agreement with the screening masses calculated in the full theory and in the effective theory.

The lightest screening mass in the 0^{++} channel was calculated in perturbation theory at next-to-leading order [118] and the corresponding result is also shown in the figure. The next-to-leading order result significantly overestimates the screening masses, while the leading order result seems to work fine. The next-to-leading order calculations also explains to some extent why the screening mass in the $\text{Tr}A_0^2$ channel is the smallest [118]. An interesting observation has been made in Ref. [115], where screening masses corresponding to the correlators of the real and imaginary parts of the Polyakov loop have been calculated. In terms of the effective 3d theory these correlators

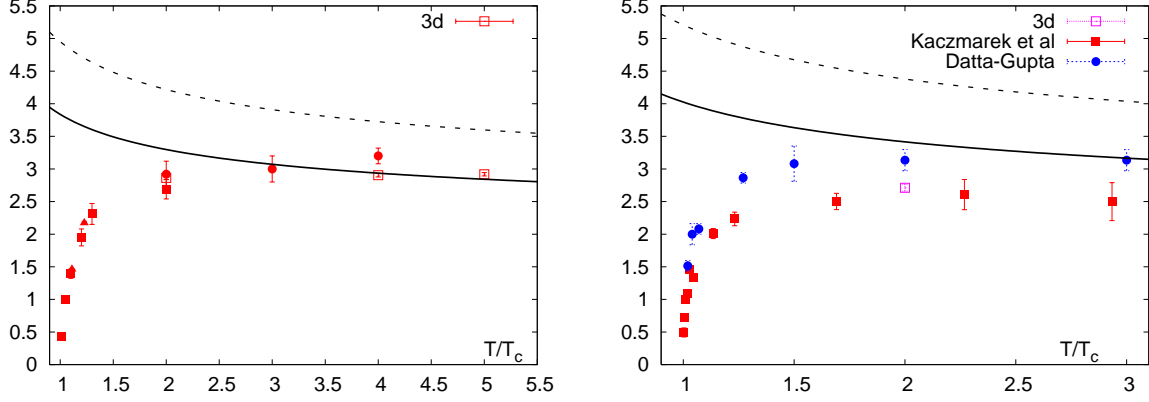


Figure 6. The lightest screening mass in 0^{++} channel calculated from the Polyakov loop correlators in $SU(2)$ gauge theory [62, 114, 119] (left) and $SU(3)$ gauge theory [61, 115] (right). Also shown as open symbols are the results of the calculations in the 3d effective theory [103, 104]. The solid and dashed lines are the perturbative predictions at leading order and next-to-leading order [118].

correspond to the correlators of $\text{Tr} A_0^2$ and $\text{Tr} A_0^3$ respectively. The ratio of the screening masses extracted from these correlators should be $2/3$ at leading order and the lattice calculations of Ref. [115] confirm this result.

4. Deconfinement : Fluctuations of conserved charges

As mentioned before due to the infamous sign problem lattice QCD Monte-Carlo simulations are not possible at non-zero quark chemical potentials. However, the pressure at non-zero chemical potentials can be evaluated using Taylor expansion. The Taylor expansion can be set up in terms of the quark chemical potentials μ_u , μ_d and μ_s , or in terms of the chemical potentials corresponding to baryon number B , electric charge Q and strangeness S of hadrons

$$\frac{p}{T^4} = \frac{1}{VT^3} \ln Z(T, \mu_u, \mu_d, \mu_s) = \sum_{ijk} \frac{1}{i!j!k!} \chi_{ijk}^{uds} \left(\frac{\mu_u}{T}\right)^i \left(\frac{\mu_u}{T}\right)^j \left(\frac{\mu_d}{T}\right)^k \quad (21)$$

$$\chi_{ijk}^{uds} = \frac{\partial^{i+j+k} p/T^4}{\partial(\mu_u/T)^i \partial(\mu_d/T)^j \partial(\mu_s/T)^k} \quad (22)$$

$$\frac{p}{T^4} = \frac{1}{VT^3} \ln Z(T, \mu_B, \mu_S, \mu_Q) = \sum_{ijk} \frac{1}{i!j!k!} \chi_{ijk}^{uds} \left(\frac{\mu_u}{T}\right)^i \left(\frac{\mu_u}{T}\right)^j \left(\frac{\mu_d}{T}\right)^k \quad (23)$$

$$\chi_{ijk}^{BQS} = \frac{\partial^{i+j+k} p/T^4}{\partial(\mu_B/T)^i \partial(\mu_Q/T)^j \partial(\mu_S/T)^k} \quad (24)$$

While Taylor expansion can be used to study the physics at non-zero baryon density the expansion coefficients are interesting on their own right as they are related to the fluctuations and correlations of conserved charges. The diagonal expansion coefficients are related to second and higher order fluctuations of conserved charges

$$\chi_2^X = \frac{1}{VT^3} \langle N_X^2 \rangle$$

$$\chi_4^X = \frac{1}{VT^3} \left(\langle N_X^4 \rangle - 3 \langle N_X^2 \rangle^2 \right) \quad (25)$$

$$\chi_6^X = \frac{1}{VT^3} \left(\langle N_X^6 \rangle - 15 \langle N_X^4 \rangle \langle N_X^2 \rangle + 30 \langle N_X^2 \rangle^3 \right), \quad (26)$$

while off-diagonal expansion coefficients are related to correlations among conserved charges, e.g.

$$\chi_{11}^{XY} = \frac{1}{VT^3} \langle N_X N_Y \rangle. \quad (27)$$

The quark chemical potentials are related to the chemical potential of baryon number, electric charge and strangeness

$$\begin{aligned} \mu_u &= \frac{1}{3} \mu_B + \frac{2}{3} \mu_Q, \\ \mu_d &= \frac{1}{3} \mu_B - \frac{1}{3} \mu_Q, \\ \mu_s &= \frac{1}{3} \mu_B - \frac{1}{3} \mu_Q - \mu_S. \end{aligned} \quad (28)$$

Therefore the expansion coefficients in quark chemical potential χ_{uds}^{jkl} are related to the hadronic ones χ_{BQS}^{jkl} . In particular, for the second order expansion coefficients we have

$$\begin{aligned} \chi_2^B &= \frac{1}{9} \left(\chi_2^u + \chi_2^d + \chi_2^s + 2\chi_{11}^{us} + 2\chi_{11}^{ds} + 2\chi_{11}^{ud} \right), \\ \chi_2^Q &= \frac{1}{9} \left(4\chi_2^u + \chi_2^d + \chi_2^s - 4\chi_{11}^{us} + 2\chi_{11}^{ds} - 4\chi_{11}^{ud} \right), \\ \chi_2^S &= \chi_2^s, \\ \chi_{11}^{BQ} &= \frac{1}{9} \left(2\chi_2^u - \chi_2^d - \chi_2^s + \chi_{11}^{us} - 2\chi_{11}^{ds} + \chi_{11}^{ud} \right), \\ \chi_{11}^{BS} &= -\frac{1}{3} \left(\chi_2^s + \chi_{11}^{us} + \chi_{11}^{ds} \right), \\ \chi_{11}^{QS} &= \frac{1}{3} \left(\chi_2^s - 2\chi_{11}^{us} + \chi_{11}^{ds} \right). \end{aligned} \quad (29)$$

Fluctuations and correlations of conserved charges are sensitive probes of deconfinement. This is because fluctuation of conserved charges are sensitive to the underlying degrees of freedom which could be hadronic or partonic. Fluctuations of conserved charges have been studied using different staggered actions [28, 56, 74, 120, 121, 122, 123, 124, 125, 126, 127, 128]. As an example in Fig. 7 I show the quadratic strangeness fluctuation as the function of the temperature calculated with *HISQ/tree* and *stout* actions. Fluctuations are suppressed at low temperatures because conserved charges are carried by massive strange hadrons (mostly kaons). They are well described by Hadron Resonance Gas (HRG) model at low temperatures. Strangeness fluctuations rapidly grow in the transition region of $T = (160 - 200)$ MeV as consequence of deconfinement. At temperatures $T > 250$ MeV strangeness fluctuations are close to unity that corresponds to the massless ideal quark gas. Similar picture can be seen in other fluctuations, in particular for light quark number fluctuation, χ_l , which is also shown in Fig. 7. The more rapid rise of χ_l in the transition region is a quark mass effect. In fact, similar quark mass dependence is seen in the HRG model. At high

temperatures the strange quark mass plays little role. In fact the difference between the strange and the light quark number susceptibilities is zero within errors. There is a good agreement between the calculations performed with *stout* and *HISQ/tree* action as the continuum limit is approached. Let me finally note that strangeness fluctuations have been calculated very recently with Wilson action for the physical values of the quark masses, and these calculations confirm the staggered result [129].

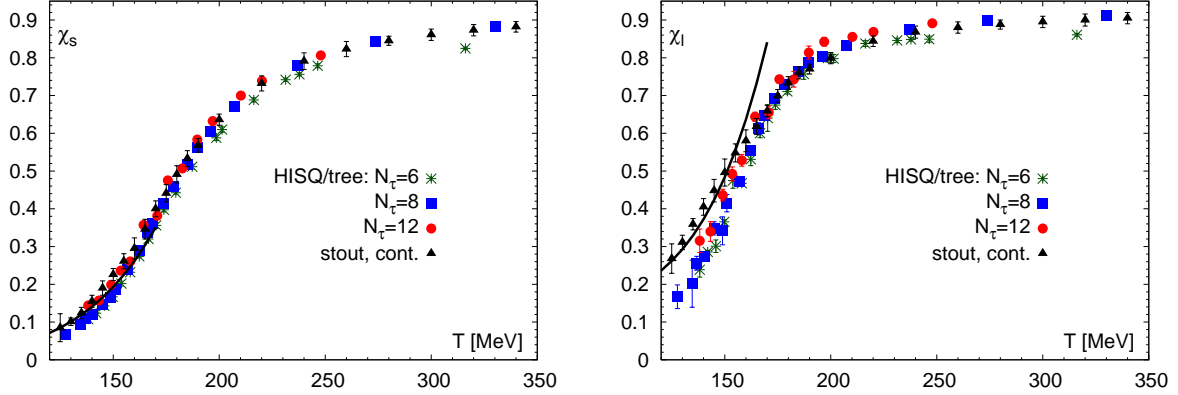


Figure 7. Strange quark number (left) and light quark number fluctuations (right) calculated with *stout* [127] and *HISQ/tree* actions [56]. The lattice results are compared with the prediction of the HRG model shown as a black line.

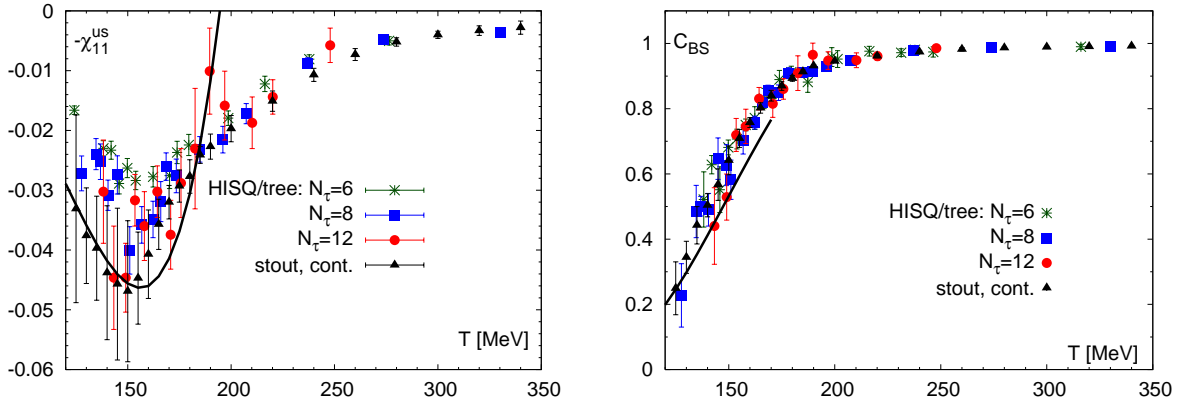


Figure 8. Quark number correlation χ_{11}^{us} (left) and C_{BS} (right) calculated with *stout* [127] and *HISQ/tree* actions [126, 128]. The lattice results are compared with the prediction of the HRG model shown as a black line.

Correlations of conserved charges, in particular quark number correlations are also sensitive to the relevant degrees of freedom. At infinitely high temperatures the correlations between different quark numbers should vanish due to the weakly interacting nature of QGP. In the high temperature region quark number correlations have been calculated in perturbation theory [130, 131, 132] and in the framework of dimensionally reduced effective theory [133]. The deviation from the ideal gas limit turned out to be quite small. At low temperatures, where hadrons are the relevant degrees of freedom

such correlations naturally arise as different quark flavors are bound in hadrons. In Fig. 8 I show the results of the lattice calculations performed with *stout* and *HISQ/tree* action for χ_{11}^{us} . These results demonstrate the expected features: at high temperatures the correlations are very small while at low temperatures they are compatible with HRG results. The fact that χ_{11}^{us} has a minimum is due to interplay between meson and baryon contributions. Mesons and baryons contribute to χ_{11}^{us} with opposite signs. At low temperatures the negative contribution from mesons dominates χ_{11}^{us} . As the temperature increases baryon contribution becomes significant and eventually the dominant one because of the larger density of states in the excited baryon sector. It is also interesting to consider the following combination

$$C_{BS} = -3\chi_{11}^{BS}/\chi_2^s = 1 + \frac{\chi_{11}^{us} + \chi_{11}^{ds}}{\chi_2^s}, \quad (30)$$

that was first introduced in Ref.[134]. The Boltzmann suppression at low temperature is canceled out in this combination and at high temperatures it should approach one. The lattice results obtained with *stout* and *HISQ/tree* actions are also shown in Fig. 8. Again, at low temperatures the lattice results are well described by HRG model, while at high temperatures C_{BS} is close to one as expected for weakly interacting quarks.

Higher order expansion coefficients have been studied in detail for $p4$ action and light quark mass $m_l = 0.1m_s$ [121]. In Fig. 9 I show the fourth and sixth order fluctuations of the electric charge. The fourth order coefficient develops a peak in the transition region and at high temperatures approaches the ideal quark gas value. The sixth order expansion coefficient has a peak around the transition temperature and becomes negative above the transition temperature. It approaches zero from below as the temperature increases as expected in the weakly interacting QGP. The sixth order expansion coefficient vanishes in the ideal gas limit as well as in the next order of perturbation theory [130]. Based on the discussion of the second order expansion coefficients we would expect that at low temperatures also the higher order expansion coefficients should be reasonably well described by HRG. However, this is not the case. As one can see from Fig. 9 the lattice results fall below the HRG prediction. This is due to the large cutoff effects related to taste symmetry breaking in the $p4$ action. Taste symmetry breaking effects lead to distortions of the hadron spectrum. If these distortions are taken into account in the HRG calculations a good agreement with the lattice data can be achieved [135, 136, 137]. The HRG model predictions with the distorted spectrum are shown in Fig. 9 as the dashed and dotted lines and are in reasonably good agreement with the lattice data. Preliminary results for the higher order expansion coefficients have been recently obtained with *HISQ/tree* action [124]. The qualitative features of these expansion coefficients remain the same, however, the location of the peak is shifted to smaller temperatures. The observed shift in the peak position is consistent with the shift in the chiral transition temperature observed in the calculations with *HISQ/tree* action [56]. The higher order expansion coefficients are sensitive to the singular part of the free energy density in the vicinity of the chiral transition temperature. Therefore I will come back to the discussion of these quantities

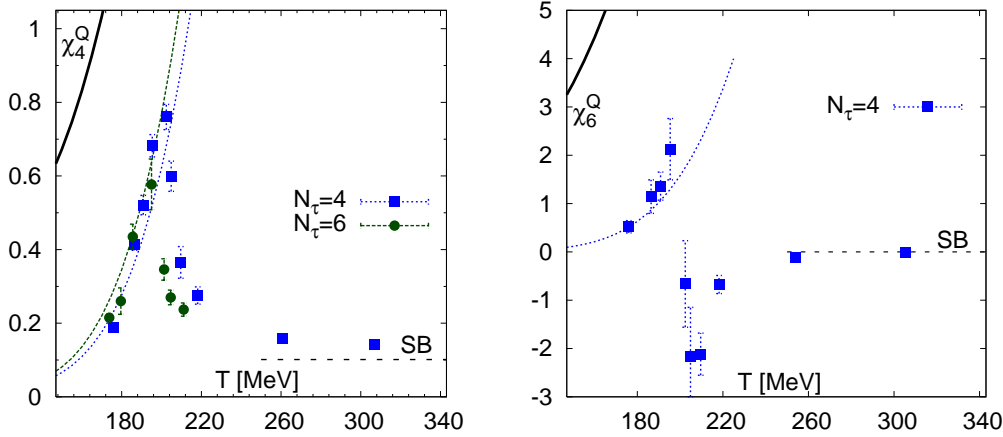


Figure 9. The fourth (left) and sixth (right) Taylor expansion coefficients for the electric charge chemical potential calculated for $p4$ action [121]. The prediction of the HRG model are shown as solid black line. The dotted and dashed lines correspond to the HRG model with the distorted hadron spectrum [136, 137].

in section 5, which is dedicated to the chiral aspects of the QCD transition.

In the high temperature region the fourth order expansion coefficient was also calculated with $p4$ action on $N_\tau = 4, 6$ and 8 lattices [123]. While no continuum extrapolation was performed the numerical data suggest that at high temperatures the fourth order expansion coefficient will approach the ideal quark gas value from below [123]. In the same study charm quark number fluctuations have been considered using partially quenched approximation, i.e. no charm quark loops. It was found that the ideal quark gas is a good approximation also in this case [123].

Finally let us compare the lattice results for quark number susceptibilities at high temperatures with the prediction of resummed perturbation theory [130, 131]. In Fig. 10 I show the lattice results for light quark number susceptibilities obtained with $p4$, *stout* and *HISQ/tree* actions compared with the resummed perturbative results. Since the difference between light and strange quark number susceptibilities is negligible for $T > 400\text{MeV}$ in the figure I also show the strange quark number susceptibilities obtained with *asqtad* action [28]. The continuum extrapolated *stout* results agree well with HTL resummed perturbative result [130]. Whereas, the $N_\tau = 8$ *asqtad* results, that are expected to be close to the continuum limit, agree with the results obtained using the next-to-leading log (NLA) approximation [131]. Clearly more lattice calculations in the high temperature limit are required to settle this issue. It is also interesting to compare the results of the lattice calculations with the results obtained in strongly coupled gauge theories using AdS/CFT correspondence. The result from AdS/CFT calculations shown in the figure as the solid black line is significantly below the lattice results ⁺.

⁺ The conserved charges considered in these calculations are not exactly the quark numbers, see discussion in Ref. [138].

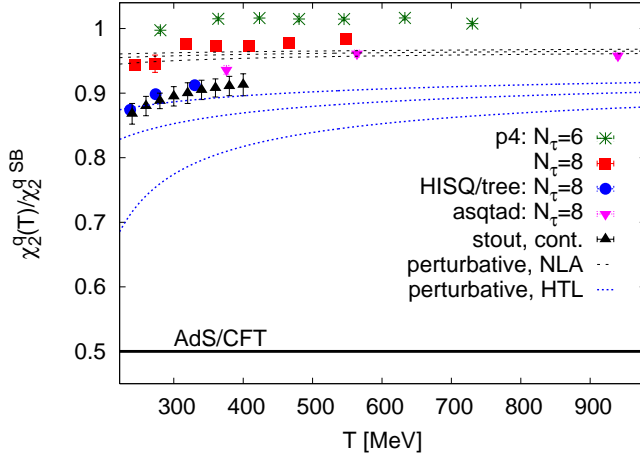


Figure 10. Quark number fluctuations calculated on the lattice with different improved staggered action and compared with the result of HTL resummed perturbation theory (dotted lines) [130] as well as the resummation that uses NLA approximation [131].

5. Chiral transition

The Lagrangian of QCD has an approximate $SU_A(3)$ chiral symmetry. This symmetry is spontaneously broken in the vacuum. The chiral symmetry breaking is signaled by non-zero expectation value of the quark or chiral condensate, $\langle \bar{\psi}\psi \rangle \neq 0$ in the massless limit. This symmetry is expected to be restored at high temperatures and the quark condensate vanishes. There is an explicit breaking of the chiral symmetry by the small value of u, d and s quark masses. While due to the relatively large strange quark mass ($m_s \simeq 100$ MeV) $SU_A(3)$ may not be a very good symmetry its subgroup $SU_A(2)$ remains a very good symmetry and is relevant for the discussion of the finite temperature transition in QCD. If the relevant symmetry is $SU_A(2)$ the chiral transition is expected to be second order for massless light (u and d) quarks belonging to the $O(4)$ universality class [18]. Recent calculations with $p4$ action confirm this pictures [139]. In other words $m_s^{phys} > m_s^{TCP}$, contrary to calculations in effective linear sigma model. This also means that for non-zero light quark masses the transition must be a crossover. The later fact seems to be supported by calculations in Ref. [27]. The $U_A(1)$ symmetry is explicitly broken in the vacuum by the anomaly but it is expected to be effectively restored at high temperatures as the non-perturbative vacuum fluctuations responsible for its breaking are suppressed at high temperatures. If the $U_A(1)$ symmetry is restored at the same temperature as the $SU_A(2)$ symmetry the transition could be first order [18]. Recent calculations with staggered as well as with domain wall fermions suggest that $U_A(1)$ symmetry gets restored at temperature that is significantly higher than the chiral transition temperature [140, 141].

For massless quarks the chiral condensate vanishes at the critical temperature T_c^0 and it is the order parameter. Therefore in the lattice studies one calculates the

chiral condensate and its derivative with respect to the quark mass, called the chiral susceptibility. For the staggered fermion formulation most commonly used in the lattice calculations these quantities can be written as follows:

$$\langle \bar{\psi}\psi \rangle_{q,x} = \frac{1}{4} \frac{1}{N_\sigma^3 N_\tau} \text{Tr} \langle D_q^{-1} \rangle, \quad (31)$$

$$\chi_{m,q}(T) = n_f \frac{\partial \langle \bar{\psi}\psi \rangle_{q,\tau}}{\partial m_l} = \chi_{q,disc} + \chi_{q,con} \quad q = l, s, \quad (32)$$

where the subscript $x = \tau$ and $x = 0$ denote the expectation value at finite and zero temperature, respectively. Furthermore, $D_q = m_q \cdot 1 + D$ is the fermion matrix in the canonical normalization and $n_f = 2$ and 1 for light and strange quarks, respectively. In Eq. (32) we made explicit that chiral susceptibility is the sum of connected and disconnected Feynman diagrams. The disconnected and connected contributions can be written as

$$\chi_{q,disc} = \frac{n_f^2}{16 N_\sigma^3 N_\tau} \left\{ \langle (\text{Tr} D_q^{-1})^2 \rangle - \langle \text{Tr} D_q^{-1} \rangle^2 \right\}, \quad (33)$$

$$\chi_{q,con} = - \frac{n_f}{4} \text{Tr} \sum_x \langle D_q^{-1}(x, 0) D_q^{-1}(0, x) \rangle, \quad q = l, s. \quad (34)$$

The disconnected part of the light quark susceptibility describes the fluctuations in the light quark condensate and is analogous to the fluctuations of the order parameter of an $O(N)$ spin model. The second term ($\chi_{q,con}$) arises from the explicit quark mass dependence of the chiral condensate and is the expectation value of the volume integral of the correlation function of the taste non-singlet scalar operator $\bar{\psi}\psi$. Let me note that in the massless limit only $\chi_{l,disc}$ diverges. In the next subsections I will discuss the temperature dependence of the chiral condensate and the chiral susceptibility as well as the role of universal scaling in the transition region.

5.1. The temperature dependence of the chiral condensate

The chiral condensate needs a multiplicative, and also an additive renormalization if the quark mass is non-zero. Therefore the subtracted chiral condensate is considered

$$\langle \bar{\psi}\psi \rangle_{sub} = \frac{\langle \bar{\psi}\psi \rangle_{l,\tau} - \frac{m_l}{m_s} \langle \bar{\psi}\psi \rangle_{s,\tau}}{\langle \bar{\psi}\psi \rangle_{l,0} - \frac{m_l}{m_s} \langle \bar{\psi}\psi \rangle_{s,0}}. \quad (35)$$

In Fig. 11 I show the results for $\langle \bar{\psi}\psi \rangle_{sub}$ calculated with *HISQ/tree* action and compared to the renormalized Polyakov loop and light quark number fluctuation discussed in relation to the deconfining transition. Interestingly, the rapid decrease in the subtracted chiral condensate happens at temperatures that are smaller than the temperatures where the Polyakov loop rises rapidly as first noticed in Ref. [52]. On the other hand the rapid change in χ_l and $\langle \bar{\psi}\psi \rangle_{sub}$ happen roughly in the same temperature region. The above results for $\langle \bar{\psi}\psi \rangle_{sub}$ obtained with *HISQ/tree* action agree well with the continuum extrapolated *stout* results.

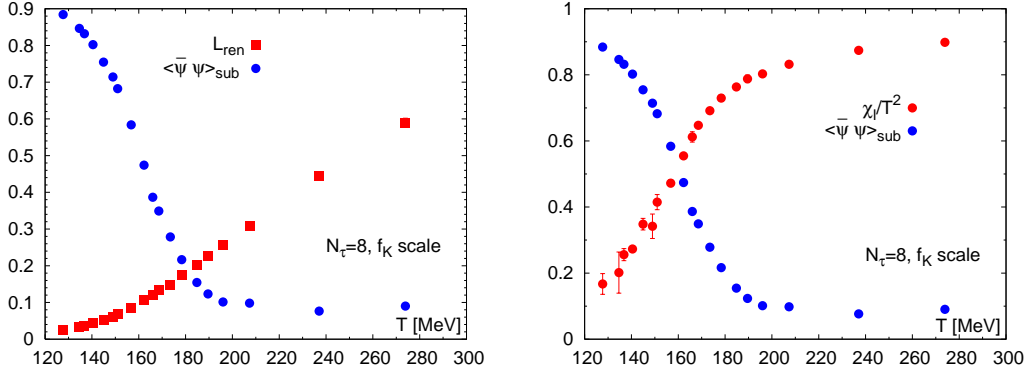


Figure 11. The subtracted chiral condensate calculated with *HISQ/tree* action on $N_\tau = 8$ lattice and compared to the renormalized Polyakov loop (left) and light quark number fluctuation (right).

Another way to get rid of the multiplicative and additive renormalization is to subtract the zero temperature condensate and multiply the difference by the strange quark mass, i.e. consider the following quantity

$$\Delta_q^R = d + n_f m_s r_1^4 (\langle \bar{\psi} \psi \rangle_{q,\tau} - \langle \bar{\psi} \psi \rangle_{q,0}), \quad q = l, s. \quad (36)$$

As before, $n_f = 2$ for the light quarks and $n_f = 1$ for the strange quark, while d is a normalization constant. The factor r_1^4 was introduced to make the combination dimensionless. It is convenient to choose the normalization constant to be the light quark condensate for $m_l = 0$ multiplied by $m_s r_1^4$. In Fig. 12 the renormalized quark condensate is shown as function of the temperature for *HISQ/tree* and *stout* actions. We see a crossover behavior for temperature of $(150 - 160)$ MeV, where Δ_l^R drops by 50%. The difference between the *stout* and *HISQ/tree* results is a quark mass effect. Calculations for *HISQ/tree* action were performed for $m_l = m_s/20$, while the *stout* calculations were done for the physical light quark masses, $m_l = m_s/27.3$. For a direct comparison with *stout* results, we need to extrapolate the *HISQ/tree* data in the light quark mass and also take care of the residual cutoff dependence in the *HISQ/tree* data. This was done in Ref. [56] and the results are shown in the figure as black diamonds demonstrating a good agreement between *HISQ/tree* and *stout* results. Contrary to Δ_l^R the renormalized strange quark condensate Δ_s^R shows only a gradual decrease over a wide temperature interval dropping by 50% only at significantly higher temperatures of about 190 MeV.

5.2. The chiral susceptibility

For a true chiral phase transition the chiral susceptibility diverges at the transition temperature. For physical value of the quark masses we expect to see a peak in the chiral susceptibility at a certain temperature that defines the crossover temperature. The chiral susceptibility also needs a multiplicative and additive renormalization. Therefore

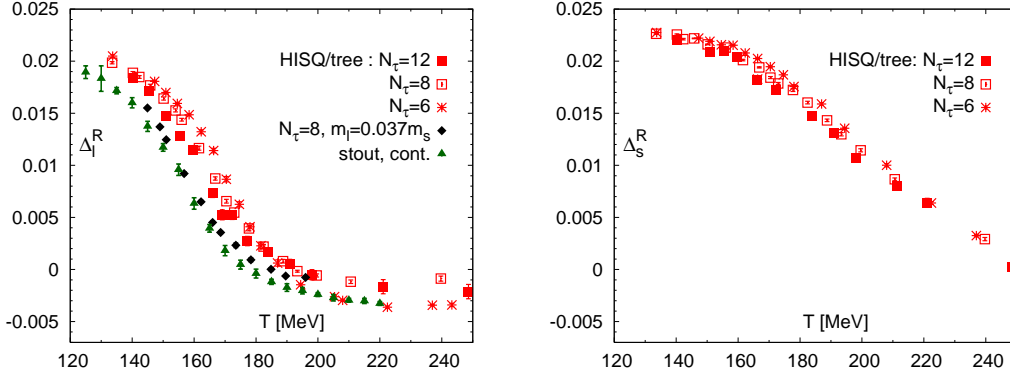


Figure 12. The renormalized chiral condensate Δ_l^R for the *HISQ/tree* action and $m_l/m_s = 0.05$ compared to the *stout* data. In the right panel, we show the renormalized strange quark condensate Δ_s^R for the *HISQ/tree* action.

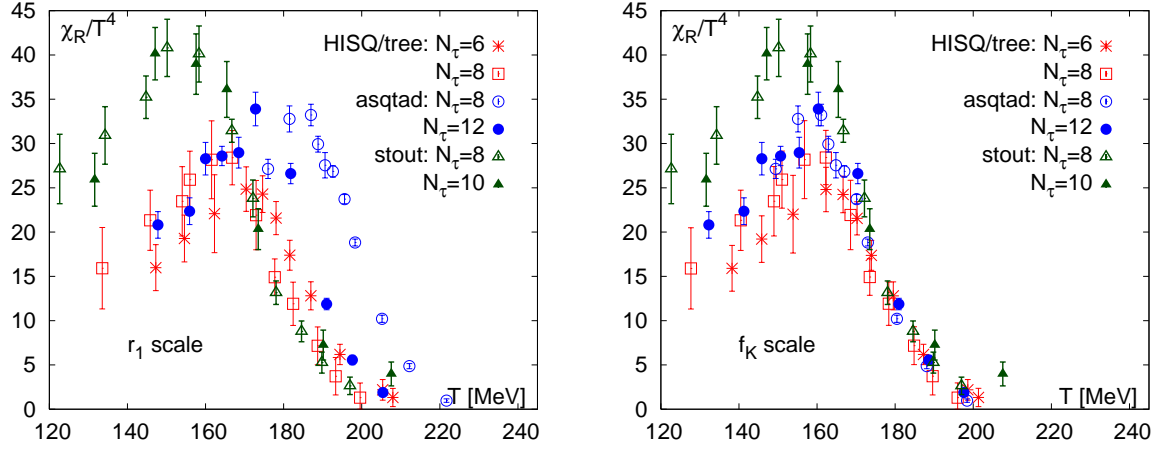


Figure 13. The renormalized chiral susceptibility χ_R for the *asqtad* and *HISQ/tree* actions obtained at $m_l = 0.05m_s$ and compared with the *stout* action results [52]. The temperature scale for *HISQ/tree* and *asqtad* actions is set using r_1 (f_K) in the left (right) panels.

the following quantity is considered

$$\frac{\chi_R(T)}{T^4} = \frac{m_s^2}{T^4} (\chi_{m,l}(T) - \chi_{m,l}(T=0)). \quad (37)$$

The numerical results for this quantity are shown in Fig. 13 for *HISQ/tree*, *asqtad* and *stout* actions *. There is a fairly good agreement between the results obtained with different actions if f_K scale is used. At low temperatures the *stout* results are above the *asqtad* and *HISQ/tree* results due to quark mass effects [56].

* In Ref. [52] the light quark mass was used instead of m_s in Eq. (37). In the comparison this was taken into account [56].

5.3. $O(N)$ scaling and the transition temperature

As discussed in the beginning of this section for physical m_s and vanishing light quark masses the transition is expected to be second order belonging to the $O(4)$ universality class in the continuum limit. At non-zero lattices spacing, however, we should expect $O(2)$ universality class as only a part of the chiral symmetry is preserved in the staggered fermion formulation. Therefore in the following we will use the term $O(N)$ universality class as referring to either $O(4)$ or $O(2)$ universality class. In the vicinity of the chiral phase transition, the free energy density may be expressed as a sum of a singular and a regular part,

$$f = -\frac{T}{V} \ln Z \equiv f_{\text{sing}}(t, h) + f_{\text{reg}}(T, m_l, m_s). \quad (38)$$

Here t and h are dimensionless couplings that control deviations from criticality. They are related to the temperature T and the light quark mass m_l as

$$t = \frac{1}{t_0} \frac{T - T_c^0}{T_c^0}, \quad h = \frac{1}{h_0} H, \quad H = \frac{m_l}{m_s}, \quad (39)$$

where T_c^0 denotes the chiral phase transition temperature, *i.e.*, the transition temperature at $H = 0$. The scaling variables t, h are normalized by two parameters t_0 and h_0 , which are unique to QCD and similar to the low energy constants in the chiral Lagrangian. These need to be determined together with T_c^0 . In the continuum limit, all three parameters are uniquely defined, but depend on the value of the strange quark mass. On the lattice they will depend on N_τ as well.

The singular contribution to the free energy density is a homogeneous function of the two variables t and h . Its invariance under scale transformations can be used to express it in terms of a single scaling variable

$$z = t/h^{1/\beta\delta} = \frac{1}{t_0} \frac{T - T_c^0}{T_c^0} \left(\frac{h_0}{H} \right)^{1/\beta\delta} = \frac{1}{z_0} \frac{T - T_c^0}{T_c^0} \left(\frac{1}{H} \right)^{1/\beta\delta} \quad (40)$$

where β and δ are the critical exponents of the $O(N)$ universality class and $z_0 = t_0/h_0^{1/\beta\delta}$. Thus, the dimensionless free energy density $\tilde{f} \equiv f/T^4$ can be written as

$$\tilde{f}(T, m_l, m_s) = h^{1+1/\delta} f_f(z) + f_{\text{reg}}(T, H, m_s), \quad (41)$$

where f_f is the universal scaling function and the regular term f_{reg} gives rise to scaling violations. This regular term can be expanded in a Taylor series around $(t, h) = (0, 0)$.

It should be noted that the reduced temperature t may depend on other parameters which do not explicitly break chiral symmetry. In particular, it depends on light and strange quark chemical potentials μ_q , which in leading order enter only quadratically,

$$t = \frac{1}{t_0} \left(\frac{T - T_c^0}{T_c^0} + \sum_{q=l,s} \kappa_q \left(\frac{\mu_q}{T} \right)^2 + \kappa_{ls} \frac{\mu_l}{T} \frac{\mu_s}{T} \right). \quad (42)$$

The transition temperature can be defined as peaks in the susceptibilities (response functions) that are second derivatives of the free energy density with respect to relevant parameters. Since there are two relevant parameters we can define three susceptibilities:

$$\chi_{m,l} = \frac{\partial^2 \tilde{f}}{\partial m_l^2}, \quad \chi_{t,l} = \frac{\partial^2 \tilde{f}}{\partial t \partial m_l}, \quad \chi_{t,t} = \frac{\partial^2 \tilde{f}}{\partial t^2}. \quad (43)$$

Thus, three different pseudo-critical temperatures $T_{m,l}$, $T_{t,l}$ and $T_{t,t}$ can be defined. In the vicinity of the critical point the behavior of these susceptibilities is controlled by three universal scaling functions that can be derived from f_f . In the chiral limit $T_{m,l} = T_{t,l} = T_{t,t} = T_c^0$. There is, however, an additional complication for $O(N)$ universality class: while $\chi_{m,l}$ and $\chi_{t,l}$ diverge at the critical point for $m_l \rightarrow 0$

$$\chi_{m,l} \sim m_l^{1/\delta-1}, \quad \chi_{t,l} \sim m_l^{(\beta-1)/\beta\delta}, \quad (44)$$

$\chi_{t,t}$ is finite because $\alpha < 0$ for $O(N)$ models ($\chi_{t,t} \sim |t|^{-\alpha}$). Therefore, one has to consider the third derivative of \tilde{f} with respect to t :

$$\chi_{t,t,t} = \frac{\partial^3 \tilde{f}}{\partial t^3}. \quad (45)$$

In the vicinity of the critical point the derivatives with respect to t can be estimated by taking the derivatives with respect to μ_l^2 , i.e. the response functions $\chi_{t,l}$ and $\chi_{t,t,t}$ are identical to the second Taylor expansion coefficient of the quark condensate and the sixth order expansion coefficient to the pressure, respectively. The former controls the curvature of the transition temperature as function of the quark chemical potential μ_q and was studied for $p4$ action using $N_\tau = 4$ and 8 lattices [142]. The later corresponds to the sixth order quark number fluctuation which is related to the deconfinement aspects of the transition. The fact that this quantity is sensitive to the chiral dynamics points to a relation between deconfining and chiral aspects of the transition. In the following I discuss the determination of the transition temperature defined as peak position of $\chi_{m,l}$, i.e. $T_c = T_{m,l}$.

5.4. Determination of the transition temperature

The $O(N)$ scaling described in the above subsection can be used to determine the pseudo-critical temperature of the chiral transition. For the study of the $O(N)$ scaling it is convenient to consider the dimensionless order parameter

$$M_b = m_s \frac{\langle \bar{\psi}\psi \rangle_l}{T^4}. \quad (46)$$

The subscript "b" refers to the fact that this is a bare quantity since the additive UV divergence is not removed. From the point of view of the scaling analysis this divergent term is just a regular contribution. For sufficiently small quark mass and in the vicinity of the transition region we can write

$$M_b(T, H) = h^{1/\delta} f_G(t/h^{1/\beta\delta}) + f_{M,reg}(T, H). \quad (47)$$

Here $f_G(z)$ is the scaling function related to f_f and was calculated for $O(2)$ and $O(4)$ spin models [143, 144, 145, 146, 147]. The regular contribution can be parametrized as [56]

$$\begin{aligned} f_{M,reg}(T, H) &= a_t(T)H \\ &= \left(a_0 + a_1 \frac{T - T_c^0}{T_c^0} + a_2 \left(\frac{T - T_c^0}{T_c^0} \right)^2 \right) H. \end{aligned} \quad (48)$$

Then we have the following behavior for the light chiral susceptibility

$$\begin{aligned} \frac{\chi_{m,l}}{T^2} &= \frac{T^2}{m_s^2} \left(\frac{1}{h_0} h^{1/\delta-1} f_\chi(z) + \frac{\partial f_{M,reg}(T, H)}{\partial H} \right), \\ \text{with } f_\chi(z) &= \frac{1}{\delta} [f_G(z) - \frac{z}{\beta} f'_G(z)]. \end{aligned} \quad (49)$$

One performs a simultaneous fit to the lattice data for M_b and $\chi_{m,l}$ treating $T_c^0, t_0, h_0, a_0, a_1$ and a_2 as fit parameters [56]. This gives a good description of the quark mass and temperature dependence of $\chi_{m,l}$ and allows to determine accurately the peak position in $\chi_{m,l}$. As an example in Fig. I show the $O(4)$ scaling fits for $N_\tau = 8$ lattice data obtained with *HISQ/tree* action. The scaling fit works quite well. Similar results have been obtained for $N_\tau = 6$ and 12 as well as for *asqtad* action on $N_\tau = 8$ and 12 lattices [56]. Furthermore, scaling fits have been performed assuming $O(2)$ universality class. The quality of these fits were similar to the $O(4)$ ones and the resulting transition temperatures turned out to be the same within statistical errors [56]. Having determined T_c for *HISQ/tree* and *asqtad* action for each N_τ a combined continuum extrapolation was performed using different assumption about the N_τ dependence of T_c . This analysis resulted in [56]:

$$T_c = (154 \pm 9) \text{ MeV}. \quad (50)$$

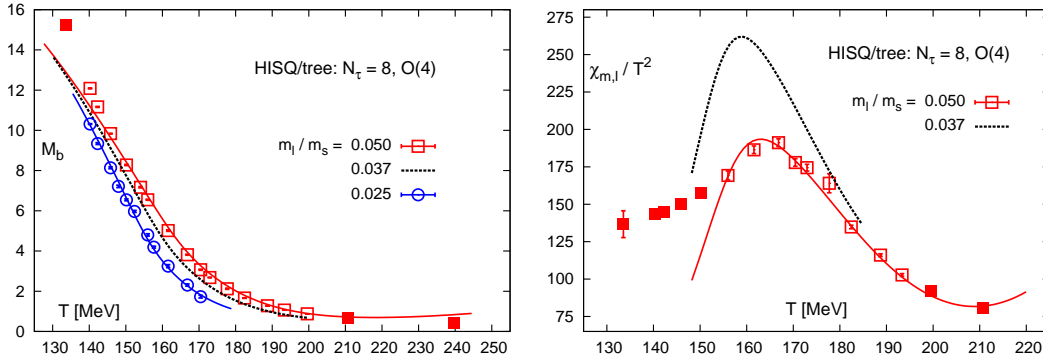


Figure 14. Scaling fits and data for the chiral condensate M_b calculated with the *HISQ/tree* action on lattices with temporal extent $N_\tau = 8$ (left) and the chiral susceptibility $\chi_{m,l}$ (right). The data for M_b at $m_l/m_s = 0.025$ and for M_b and $\chi_{m,l}$ at $m_l/m_s = 0.05$ are fit simultaneously using the $O(4)$ scaling Ansatz. The points used in the scaling fits are plotted using open symbols. The dotted lines give the data scaled to the physical quark masses.

The analysis also demonstrated that *HISQ/tree* and *asqtad* action give consistent results in the continuum limit. The Budapest-Wuppertal collaboration found $T_c = 147(2)(3)\text{MeV}$, $157(3)(3)\text{MeV}$ and $155(3)(3)\text{MeV}$ defined as peak position in χ_R , inflection points in $\langle\bar{\psi}\psi\rangle_{sub}$ and Δ_l^R respectively [74]. These agree with the above value within errors.

5.5. The chiral transition temperature for small chemical potential

The scaling analysis described in the above subsection is also useful for the determination of the chiral transition temperature for small quark chemical potential. Also for non-zero quark chemical potential the phase transition happens at $t = 0$. Together with Eq. (42) this implies that the μ_q dependence of the chiral phase transition temperature is given by

$$T_c^0(\mu_q) = T_c^0(0) - \kappa_l \left(\frac{\mu_l}{T_c^0} \right)^2 + \mathcal{O} \left(\left(\frac{\mu_l}{T_c^0} \right)^4 \right). \quad (51)$$

The value of κ_l can be determined through lattice calculations of the mixed susceptibility $\chi_{t,l}$ [142]. The mixed susceptibility can be expressed in terms of the derivative of the scaling function of the order parameter $f_G(z)$

$$\frac{\chi_{t,l}}{T} = \frac{2\kappa_l T}{t_0 m_s} h^{-(1-\beta)/(\beta\delta)} f'_G(z). \quad (52)$$

Calculations with $p4$ action on $N_\tau = 4$ and 8 lattices of the mixed susceptibility have been performed for several quark masses and resulted in the value [142]

$$\kappa_l = 0.059(2)(4). \quad (53)$$

This result for the curvature of the critical line is about factor of two larger than the result obtained in Ref. [148, 149] using multi-parameter re-weighting technique. On the other hand it is consistent with the results obtained using the imaginary chemical potential technique [150, 151, 152].

Finally let me mention that the study of the mixed susceptibility allows to estimate the width of the chiral crossover for physical light quark masses. The pseudo-critical temperatures $T_{t,l}$ and $T_{m,l}$ are determined by the peak positions z_p of the $f'_G(z)$ and $f_\chi(z)$ when scaling violations are neglected. Namely,

$$\frac{T_{p,l} - T_c^0}{T_c^0} = \frac{z_p}{z_0} H^{1/(\beta\delta)}, \quad p = m, t. \quad (54)$$

The peak positions of the above scaling functions for $O(4)$ model have been determined to be $z_p = 0.74(4)$ and $1.374(30)$ respectively [147]. From these and from the values of z_0 and T_c^0 published in Ref. [142] for $p4$ action one can estimate $T_{m,l}$ to be higher than $T_{t,l}$ by 4MeV and 2MeV for physical value of the light quark mass for $N_\tau = 8$ and 4 respectively. These estimates are reliable since the scaling violations were found to be small for $p4$ action [142]. In particular, the combination $-m_s t_0 h^{(1-\beta)/(\beta\delta)} \chi_{t,l}/T^2$ as function of z has a peak at $z \simeq 0.74$ [142]. It remains to be seen how this picture changes when *HISQ/tree* action is used.

6. Equation of State

The equation of state has been calculated using different improved staggered fermion actions *p4*, *asqtad*, *stout* and *HISQ/tree*. The calculation of thermodynamic observables proceeds through the calculation of the trace of the energy momentum tensor, $\epsilon - 3p$, also known as trace anomaly or interaction measure. This is due to the fact that this quantity can be expressed in terms of expectation values of local gluonic and fermionic operators, (see e.g. Ref. [122]). Different thermodynamic observables can be obtained from the interaction measure through integration of the trace anomaly \ddagger . The pressure can be written as

$$\frac{p(T)}{T^4} - \frac{p(T_0)}{T_0^4} = \int_{T_0}^T \frac{dT'}{T'^5} (\epsilon - 3p). \quad (55)$$

The lower integration limit T_0 is chosen such that the pressure is exponentially small there. Furthermore, the entropy density can be written as $s = (\epsilon + p)/T$. Since the interaction measure is the basic thermodynamic observable in the lattice calculations it is worth to discuss its properties more in detail. In Fig. 15 (left panel) I show the results of calculation with *p4* and *asqtad* actions using $N_\tau = 6$ and 8 lattices and light quark masses $m_l = m_s/10$, where m_s is the physical strange quark mass. These calculations correspond in the continuum limit to the pion mass of 220MeV and 260MeV for *p4* and *asqtad* respectively. The interaction measure shows a rapid rise in the transition region and after reaching a peak at temperatures of about 200MeV decreases. Cutoff effects (i.e. N_τ dependence) appears to be the strongest around the peak region and decrease at high temperatures. For temperatures $T < 270$ MeV calculations with *p4* and *asqtad* actions have been extended to smaller quark masses, $m_l = m_s/20$, that correspond to the pion mass of about 160MeV in the continuum limit [154, 155]. It turns out that the quark mass dependence is negligible for $m_l < m_s/10$. Furthermore, for *asqtad* action calculations have been extended to $N_\tau = 12$ lattices [155, 156]. The trace anomaly was calculated with *HISQ/tree* action on lattices with temporal extent $N_\tau = 6$ and 8 and $m_l = m_s/20$ [155, 156] (corresponding to $m_\pi = 160$ MeV in the continuum limit). Finally, calculation of the trace anomaly and the equation of state was performed with *stout* action using $N_\tau = 4, 6, 8, 10$ and 12 and physical light quark masses [153]. Using the lattice data from $N_\tau = 6, 8, 10$ a continuum estimate for different quantities was given [153]. In Fig. 15 (right panel) the results of different lattice calculations of $\epsilon - 3p$ corresponding to the pion masses close to the physical value are summarized. I also compare the lattice results with the parametrization s95p-v1 of $\epsilon - 3p$. This parametrization combines lattice QCD results of Refs. [87, 122] at high temperatures with hadron resonance gas model (HRG) at low temperatures ($T < 170$ MeV) [135]. At low temperatures there is a fair agreement between the results obtained with *stout* action and the results obtained with *HISQ/tree* action as well as with *asqtad* action for $N_\tau = 12$. All these lattice results are slightly above the HRG curve. For $N_\tau = 8$ cutoff effects are significant for *asqtad* and *p4* action. As the result the corresponding lattice

\ddagger A somewhat different approach was used in Ref. [153]

data fall below the HRG (s95p-v1) curve at low temperatures. When cutoff effects in the hadron spectrum are taken into account in the HRG model a good agreement between the $p4$ data and HRG result can be achieved [135]. The height of the peak in $\epsilon - 3p$ is the same for $asqtad$ and $HISQ/tree$ actions. At the same time it is smaller for the $stout$ action. Since the dominant cutoff effects of order a^2T^2 are eliminated, the N_τ -dependence is expected to be small for $p4$, $asqtad$ and $HISQ/tree$ action at high temperatures. We see that for $T > 250\text{MeV}$ all these lattice actions lead to similar results. At temperatures above 350MeV we also see a good agreement with the $stout$ results.

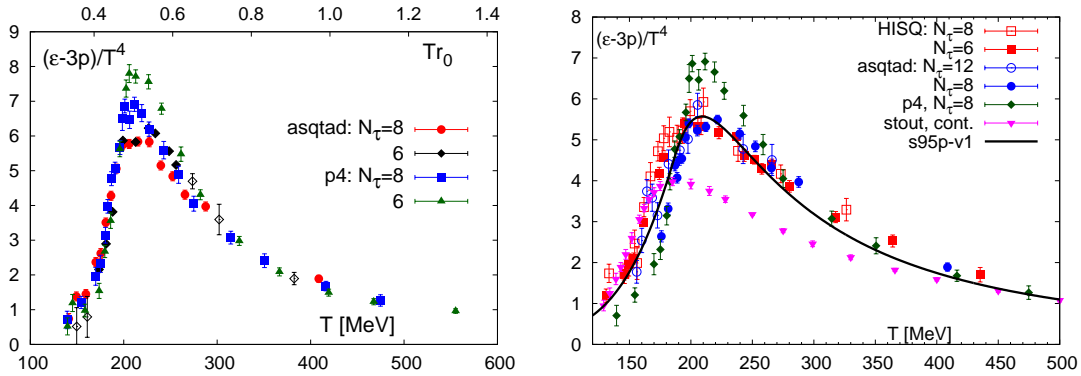


Figure 15. The interaction measure calculated with $m_l = m_s/10$ and $p4$ and $asqtad$ actions [122] (left) and with $m_l = m_s/20$ for $p4$ action [154] as well as with $HISQ/tree$ and $asqtad$ actions [155]. Also shown in the figure are the continuum estimates obtained with $stout$ action and the parametrization based on hadron resonance gas (HRG) model [135].

The pressure, the energy density and the entropy density are shown in Fig. 16. The energy density shows a rapid rise in the temperature region (170–200) MeV and quickly approaches about 90% of the ideal gas value. The pressure rises less rapidly but at the highest temperature it is also only about 15% below the ideal gas value. In the previous calculations with the $p4$ action it was found that the pressure and the energy density are below the ideal gas value by about 25% at high temperatures [157]. A possible reason for this larger deviation could be the fact that the quark masses used in this calculation were fixed in units of temperature instead being tuned to give constant meson masses as lattice spacing is decreased. As discussed in Ref. [158] this could reduce the pressure by 10 – 15% at high temperatures. In Fig. 16 I also show the entropy density divided by the corresponding ideal gas value and compare the results of lattice calculations with resummed perturbative calculation [159, 160] as well as with the predictions from AdS/CFT correspondence for the strongly coupled supersymmetric Yang-Mills theory [161]. The later is considerably below the lattice results. Note that the pressure, the energy density and the trace anomaly have also been recently discussed in the framework of resummed perturbative calculations which seem to agree with lattice data quite well at high temperatures[162].

The difference between the *stout* action and the *p4* and *asqtad* actions for the trace anomaly translates into the differences in the pressure and the energy density. In particular, the energy density is about 20% below the ideal gas limit for the *stout* action.

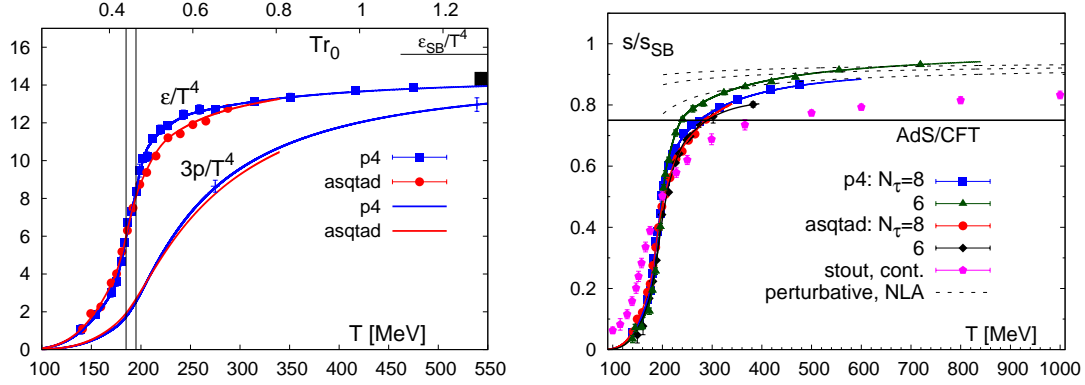


Figure 16. The energy density and the pressure as function of the temperature (left), and the entropy density divided by the corresponding ideal gas value (right). The dashed lines in the right panel correspond to the resummed perturbative calculations while the solid black line is the AdS/CFT result.

7. Meson correlators and spectral functions

In-medium meson properties as well as some transport coefficients are encoded in meson spectral functions. Medium modification of meson spectral functions can serve as diagnostic tools of the medium created in heavy ion collisions. For example, the excess in the low mass dilepton rate can be related to the modification of the light vector meson spectral function (see Ref. [163] for a recent review). The suppression of quarkonium yield was suggested by Matsui and Satz as signal for QGP formation in heavy ion collisions [164]. Studying quarkonium melting in QGP and the consequent suppression of the quarkonium yield is subject of a large experimental and theoretical effort (see Refs. [165, 166, 167, 168] for reviews).

The spectral function $\sigma_H(\omega, \vec{p})$ for a given meson channel H in a system at temperature T can be defined through the Fourier transform of the real time two point functions $D^>$ and $D^<$ or equivalently as the imaginary part of the Fourier transformed retarded correlation function [57],

$$\begin{aligned}\sigma_H(\omega, \vec{p}) &= \frac{1}{2\pi} (D_H^>(\omega, \vec{p}) - D_H^<(\omega, \vec{p})) \\ &= \frac{1}{\pi} \text{Im} D_H^R(\omega, \vec{p}) \\ D_H^{>(<)}(\omega, \vec{p}) &= \int_{-\infty}^{\infty} dt \int d^3x e^{i\omega t - i\vec{p} \cdot \vec{x}} D_H^{>(<)}(t, \vec{x})\end{aligned}\tag{56}$$

$$\begin{aligned}D_H^>(t, \vec{x}) &= \langle J_H(t, \vec{x}), J_H(0, \vec{0}) \rangle \\ D_H^<(t, \vec{x}) &= \langle J_H(0, \vec{0}), J_H(t, \vec{x}) \rangle, t > 0\end{aligned}\tag{57}$$

Γ	$^{2S+1}L_J$	J^{PC}	$u\bar{u}$	$c\bar{c}(n=1)$	$c\bar{c}(n=2)$	$b\bar{b}(n=1)$	$b\bar{b}(n=2)$
γ_5	1S_0	0^{-+}	π	η_c	η'_c	η_b	η'_b
γ_s	3S_1	1^{--}	ρ	J/ψ	ψ'	$\Upsilon(1S)$	$\Upsilon(2S)$
$\gamma_s\gamma_{s'}$	1P_1	1^{+-}	b_1	h_c		h_b	
1	3P_0	0^{++}	a_0	χ_{c0}		$\chi_{b0}(1P)$	$\chi_{b0}(2P)$
$\gamma_5\gamma_s$	3P_1	1^{++}	a_1	χ_{c1}		$\chi_{b1}(1P)$	$\chi_{b1}(2P)$
		2^{++}		χ_{c2}		$\chi_{b2}(1P)$	$\chi_{b2}(2P)$

Table 1. Meson states in different channels for light, charm and bottom quarks.

In essence σ_H is the Fourier transformation of the thermal average of the commutator $[J(x), J(0)]$.

In the present paper we study local meson operators of the form

$$J_H(t, x) = \bar{q}(t, \vec{x}) \Gamma_H q(t, \vec{x}) \quad (58)$$

with $q(t, \vec{x})$ is the quark field operator and

$$\Gamma_H = 1, \gamma_5, \gamma_\mu, \gamma_5\gamma_\mu, \gamma_\mu\gamma_\nu \quad (59)$$

for scalar, pseudo-scalar, vector, axial-vector and tensor channels. The relation of these quantum number channels to different meson states is given in Tab. 1. In the vector channel I will use the subscript V to denote the sum over all four components, while the subscript ii will be used for the spatial components of the vector correlators and spectral functions.

The correlators $D_H^{>(<)}(t, \vec{x})$ satisfy the well-known Kubo-Martin-Schwinger (KMS) condition [57]

$$D_H^{>}(t, \vec{x}) = D_H^{<}(t + i/T, \vec{x}). \quad (60)$$

Inserting a complete set of states and using Eq. (60), one gets the expansion

$$\begin{aligned} \sigma_H(\omega, \vec{p}) &= \frac{1}{Z} \sum_{m,n} e^{-E_n/T} \times \\ &\langle n | J_H(0) | m \rangle|^2 \left(\delta^4(p_\mu + k_\mu^n - k_\mu^m) - \delta^4(p_\mu + k_\mu^m - k_\mu^n) \right) \end{aligned} \quad (61)$$

where Z is the partition function, $k^{n(m)}$ refers to the four-momenta of the state $|n(m)\rangle$ and $p_\mu = (\omega, \vec{p})$.

A stable meson state contributes a δ function-like peak to the spectral function:

$$\sigma_H(\omega, \vec{p}) = |\langle 0 | J_H | H \rangle|^2 \epsilon(\omega) \delta(p^2 - M_H^2), \quad (62)$$

where M_H is the mass of the state and $\epsilon(p_0)$ is the sign function. For a quasi-particle in the medium one gets a smeared peak, with the width being the thermal width. As one increases the temperature the width increases and at sufficiently high temperatures, the contribution from the meson state in the spectral function may be sufficiently broad. At some point it is not very meaningful to speak of it as a well defined state any more. The spectral function as defined in Eq. (61) can be directly accessible by high energy

heavy ion experiments. More precisely, the spectral function for the vector current is directly related to the differential thermal cross section for the production of dilepton pairs [169, 170]:

$$\left. \frac{dW}{d\omega d^3p} \right|_{\vec{p}=0} = \frac{5\alpha_{em}^2}{27\pi^2} \frac{1}{\omega^2(e^{\omega/T} - 1)} \sigma_V(\omega, \vec{p}). \quad (63)$$

Then presence or absence of a bound state in the spectral function will manifest itself in the peak structure of the differential dilepton rate.

In finite temperature lattice calculations, one calculates Euclidean time propagators, usually projected to a given spatial momentum:

$$G_H(\tau, \vec{p}) = \int d^3x e^{i\vec{p}\cdot\vec{x}} \langle T_\tau J_H(\tau, \vec{x}) J_H(0, \vec{0}) \rangle \quad (64)$$

This quantity is an analytical continuation of $D_H^>(x_0, \vec{p})$

$$G_H(\tau, \vec{p}) = D_H^>(-i\tau, \vec{p}). \quad (65)$$

The KMS condition implies the following relation for the Fourier transforms of $D_H^<$ and $D_H^>$

$$D_H^<(\omega, \vec{p}) = D_H^>(-\omega, \vec{p}) = e^{-\omega/T} D_H^>(\omega, \vec{p}). \quad (66)$$

This leads to a relation between $D^>(\omega, \vec{p})$ and the spectral function

$$D_H^>(\omega, \vec{p}) = 2\pi\sigma_H(\omega, \vec{p})e^{\omega/T}/(e^{\omega/T} - 1). \quad (67)$$

Using this and Eq. (65) we get the following integral representation for the Euclidean time correlator

$$G_H(\tau, \vec{p}) = \int_0^\infty d\omega \sigma_H(\omega, \vec{p}) K(\omega, \tau),$$

$$K(\omega, \tau) = \frac{\cosh(\omega(\tau - 1/2T))}{\sinh(\omega/2T)}. \quad (68)$$

This equation is the basic equation for extracting the spectral function from meson correlators. Equation (68) is valid in the continuum. Formally the same spectral representation can be written for the Euclidean correlator calculated on the lattice $G_H^{lat}(\tau, \vec{p})$. The corresponding spectral function, however, will be distorted by the effect of the finite lattice spacing, in particular, the spectral function is zero above certain energy $\omega > \omega_{max}$. These distortions have been calculated in the free theory [171, 172]. When discussing the numerical results in following sections the subscript H denoting different channels for meson correlators and spectral functions will be omitted unless stated otherwise.

To get some information on the spectral functions from lattice QCD the corresponding Euclidean time correlation functions have to be calculated at as many separations in the time direction as possible, i.e. one should use large N_τ . One way to accomplish this task with available computer resources is to use anisotropic lattices, i.e. lattices with different spacings a_t and a_s in time and space directions, such that $\xi = a_t/a_s > 1$. In addition one also often uses the quenched approximation for studying spectral functions on the lattice.

The low frequency limit of the vector spectral function gives information about the transport coefficients of the medium, namely the electric conductivity and the heavy quark diffusion constant. Other transport coefficients, such as the shear and bulk viscosity are related to the correlation functions of gluonic operators (see Ref. [173] for a review). The quark flavor diffusion constant \mathcal{D}_q can be defined through the time derivative of the quark number density in the rest frame of the thermal system as follows

$$\partial_t n_q = \mathcal{D}_q \nabla^2 n_q + \mathcal{O}(\nabla^3). \quad (69)$$

This equation holds for small deviation from thermal equilibrium. The quark flavor diffusion constant can be determined from the spatial component of the vector spectral function as follows

$$\mathcal{D}_q = \frac{1}{3\chi_q} \lim_{\omega \rightarrow 0} \frac{\sigma_{ii}(\omega)}{\omega}, \quad (70)$$

here χ_q is the quark number susceptibility. The electric conductivity is related to the correlation function of electric currents

$$J_\mu^{em} = \sum_f Q_f \bar{q}_f(t, \vec{x}) \gamma_\mu q_f(t, \vec{x}), \quad (71)$$

with Q_f being the electric charge of quark flavor f . The correlator of the electromagnetic current receives contribution from quark line connected and quark line disconnected diagrams. At high temperatures the contribution from the disconnected diagrams is small. For degenerate quark flavors the electric conductivity can be written as [174]

$$\zeta = \chi_q \left[\left(\sum_f Q_f \right)^2 \mathcal{D}_{q, disc} + \left(\sum_f Q_f^2 \right) \mathcal{D}_{q, con} \right], \quad \mathcal{D}_q = \mathcal{D}_{q, con} + \mathcal{D}_{q, dis}. \quad (72)$$

For degenerate u , d and s quarks the disconnected contribution vanishes since $\sum_{f=u,d,s} Q_f = 0$. The quark flavor diffusion coefficient for single heavy quark flavor ($m_q \gg T$) is called the heavy quark diffusion constant D . It is related to the momentum drag coefficient η in the Langevin dynamics of heavy quarks [175]:

$$D = \frac{T}{m_q \eta}. \quad (73)$$

In lattice QCD one also calculates meson correlation function in one of the spatial directions, say z

$$G(z, T) = \int dx dy \int_0^{1/T} d\tau \langle J(x, y, z, \tau) J(0, 0, 0, 0) \rangle. \quad (74)$$

The spatial correlation function is related to the meson spectral function at non-zero spatial momentum

$$G(z, T) = \int_{-\infty}^{\infty} dp_z e^{ip_z z} \int_0^{\infty} d\omega \frac{\sigma(\omega, p_z, T)}{\omega}. \quad (75)$$

Thus the temperature dependence of the spatial correlation function also provides information about the temperature dependence of the spectral function. Medium effects are expected to be the largest at distances which are larger than $1/T$. At these distances

$G(z, T)$ decays exponentially and this exponential decay is governed by a screening mass M_{scr} . If there is a lowest lying meson state of mass M , i.e. the spectral function can be well approximated by Eq. (62), then the long distance behavior of the spatial meson correlation function is determined by the meson mass, i.e. $M_{scr} = M$. At very high temperatures the quark and anti-quark are not bound and the meson screening mass is given by $2\sqrt{(\pi T)^2 + m_q^2}$, where m_q is the quark mass and πT is the lowest Matsubara frequency. Therefore, a detailed study of spatial meson correlators and screening masses can provide some information about the melting of meson states at high temperatures.

One would like to obtain the spectral functions through lattice calculation of the temporal meson correlation function. The obvious difficulty in the reconstruction of the spectral function from Eq. (68) is the fact that the Euclidean correlator is calculated only at $\mathcal{O}(10)$ data points on the lattice, while for a reasonable discretization of the integral in Eq. (68) we need $\mathcal{O}(100)$ degrees of freedom. The problem can be solved using Bayesian analysis of the correlator, where one looks for a spectral function which maximizes the conditional probability $P[\sigma|DH]$ of having the spectral function σ given the data D and some prior knowledge H (for reviews see [176, 177]). Different Bayesian methods differ in the choice of the prior knowledge. One version of this analysis which is extensively used in the literature is the *Maximum Entropy Method* (MEM) [178, 179]. It has been used to study different correlation functions in QCD [179, 176, 180, 181, 182, 183, 184, 185, 186, 187, 188, 189, 190, 191, 192, 193]. In this method the basic prior knowledge is the positivity of the spectral function and the prior knowledge is given by the Shannon - Janes entropy

$$S = \int d\omega \left[\sigma(\omega) - m(\omega) - \sigma(\omega) \ln\left(\frac{\sigma(\omega)}{m(\omega)}\right) \right]. \quad (76)$$

The real function $m(\omega)$ is called the default model and parametrizes all additional prior knowledge about the spectral functions, e.g. such as the asymptotic behavior at high energy [179, 176]. For MEM the conditional probability can be written as

$$P[\sigma|DH] = \exp\left(-\frac{1}{2}\chi^2 + \alpha S\right), \quad (77)$$

with χ^2 being the standard likelihood function and α is a real parameter.

Early results on meson spectral functions obtained with MEM gave a number of unexpected results. In particular, the MEM analysis of the charmonium correlators calculated in quenched QCD suggested that 1S charmonium states can survive in QGP up to temperatures as high as $1.6T_c$ (see e.g. [188]). Here T_c is the deconfinement phase transition temperature of $SU(3)$ gauge theory. This is in odds with the expected medium modification of the heavy quark potential that in addition to the effects of color screening also includes an imaginary part [73, 194]. In fact, many potential model calculations indicate melting of 1S charmonium state in the deconfined medium [195, 196, 197, 198, 199, 200]. Furthermore, even in the light meson spectral functions peak structures have been observed [185]. It is not clear to what extent these correspond to physical effects or are artifacts of the calculations. Next we will consider the

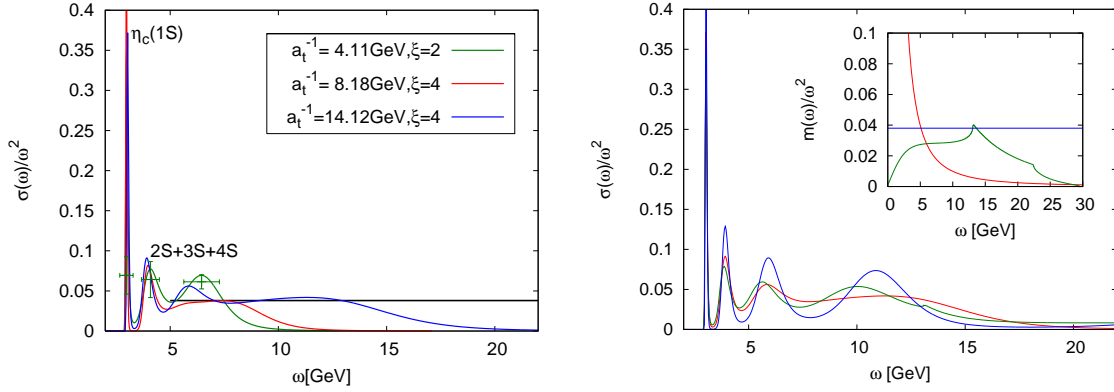


Figure 17. The spectral function in the pseudo-scalar channel calculated for several lattice spacings (left). The default model dependence of the spectral function calculated on $24^3 \times 160$ lattice (right). The inset in the right panel shows the different default models used in the analysis.

determination of the meson spectral function separately for the case of heavy quarks and light quarks.

7.1. Quarkonium spectral functions at zero temperature

The best way to understand the structure of meson spectral functions and the issues related to their determination on the lattice is to consider the case of heavy quarkonium at zero temperature. Charmonium correlation functions have been studied in detail in Ref. [201] using quenched anisotropic lattices and the so-called Fermilab formulations for heavy quarks [202]. Spectral functions have been extracted using MEM. The spectral functions in the pseudo-scalar channel calculated at three lattice spacings are shown in Fig. 17. The first peak corresponds to the ground state, $\eta_c(1S)$. The second peak is actually the combination of several excited states, since MEM cannot resolve individual excited meson states due to the small splitting between them [201]. For $\omega > 5$ GeV we see the continuum. The spectral function becomes zero above certain energy ω due to the presence of finite lattice as expected in the free theory. In Fig. 17 I also show the spectral function calculated for different default models $m(\omega)$. The default model dependence is small for $\omega < 5$ GeV, while above that energy it is significant due to the fact that there are only very few data points that carry information about the spectral function in that region. As the temperature increases the number of data points available for the analysis as well as the maximal extent of the time direction $\tau_{max} = 1/(2T)$ become smaller. To demonstrate this point in Fig. 18 I show the zero temperature charmonium spectral function calculated with different number of data points and τ_{max} that are characteristic for temperatures corresponding to QGP. As τ_{max} decreases MEM loses the ability to reconstruct the peak corresponding the excited states and the ground state peak is significantly broadens. For $\tau_{max} = 0.22$ fm even the position of the ground state peak is not reproduced correctly. Furthermore, the shape of the spectral functions, in

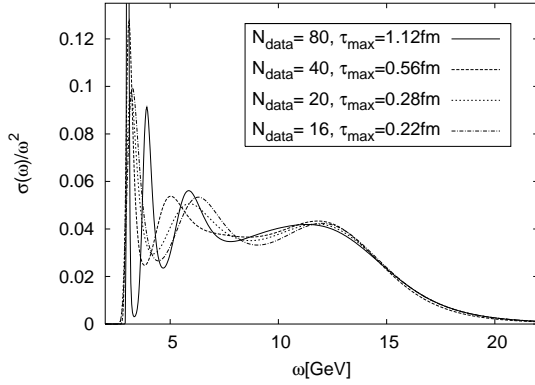


Figure 18. The dependence of the pseudo-scalar spectral function on τ_{max} .

particular, the presence of the ground state peak also becomes sensitive to the default model.

Since the analysis of the quarkonium spectral functions using MEM turns out to be quite complicated already in the zero temperature limit, it is important to understand the temperature dependence of the quarkonium correlation functions and try to identify possible sources of the temperature dependence that are related to melting of the bound states. From Eq. (68) it is clear that the temperature dependence of the meson correlation functions comes from two sources: the trivial temperature dependence of the integration kernel $K(\tau, \omega)$ and the temperature dependence of the spectral function $\sigma(\omega, T)$. To get rid of the first trivial temperature dependence one can consider the reconstructed correlation function

$$G_{\text{rec}}(\tau, T) = \int_0^\infty d\omega \sigma(\omega, T=0) K(\omega, \tau). \quad (78)$$

If the spectral function does not change across the deconfinement transition $G(\tau, T)/G_{\text{rec}}(\tau, T)$ should be unity. Deviations of this ratio from unity indicate temperature dependence of the spectral functions. The ratio $G(\tau, T)/G_{\text{rec}}(\tau, T)$ was first studied in Ref. [189] and subsequently in Refs. [190, 193, 201, 203]. It was found that in the pseudo-scalar channel this ratio stays close to one and shows only small temperature dependence. This seemed to support the conclusion based on the spectral functions extracted from MEM that ground state charmonium survives in the deconfined phase up to temperatures $1.6T_c$. In the scalar and axial-vector channels large temperature dependence in $G(\tau, T)/G_{\text{rec}}(\tau, T)$ was observed. This was interpreted as melting of 1P charmonium states and fitted well into the expected picture of sequential melting. However, this conclusion was premature. In the deconfined phase there is an additional contribution to the spectral functions at very low frequency. This can be easily seen by calculating the spectral function in the free theory. In addition to the contribution to the spectral function that starts at twice the heavy quark mass there is a contribution proportional to $\omega\delta(\omega)$ in all but the pseudo-scalar channel [172]. The delta function is smeared once the interactions of the heavy quarks with the medium are taken into account. In particular, in the vector channel, where this low ω structure

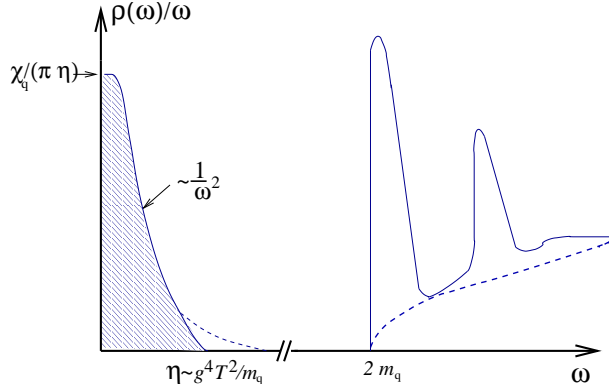


Figure 19. The schematic structure of the vector spectral function for heavy quarks.

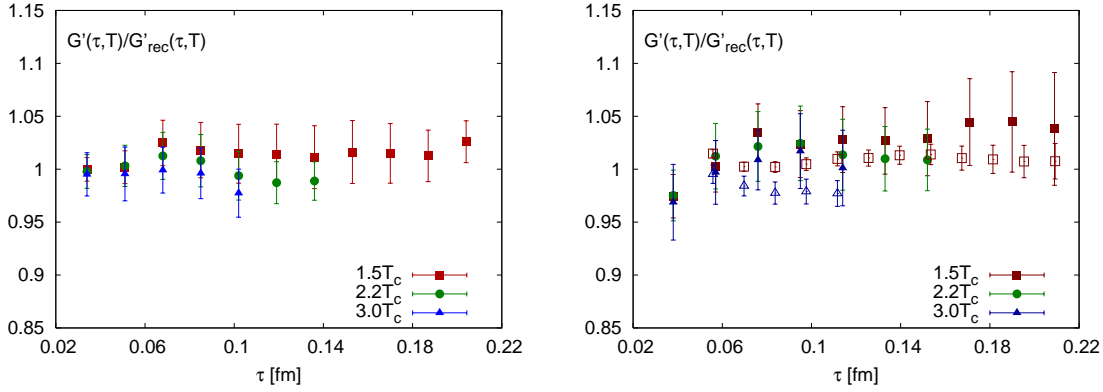


Figure 20. The ratio of the derivatives of the charmonium correlators to the corresponding reconstructed correlators for the pseudo-scalar (left) and scalar (right) channels [205].

is related to the heavy quark diffusion we have [204]

$$\omega \delta(\omega) \rightarrow \frac{1}{\pi} \frac{\eta \omega}{\omega^2 + \eta^2}, \quad \eta = T/(Dm_q), \quad (79)$$

with m_q being the heavy quark mass and D being the heavy quark diffusion constant. The schematic structure of the spectral functions is shown in Fig. 19. The area under the transport peak is given by the quark number susceptibility χ_q . For large quark mass the transport peak is narrow and is well separated from the high energy part of the spectral function that corresponds to bound states and/or unbound heavy quark anti-quark pairs. We expect similar structure in the spectral function in other channels as well. Thus we can write

$$\sigma(\omega, T) = \sigma_{low}(\omega, T) + \sigma_{high}(\omega, T) \quad (80)$$

$$G(\tau, T) = G_{low}(\tau, T) + G_{high}(\tau, T). \quad (81)$$

Since the peak at low ω is narrow we expect that the derivative of $G_{low}(\tau, T)$ with respect of τ is small, $G'_{low}(\tau, T) \simeq 0$. In Fig. 20 I show the ratio of the derivatives $G'(\tau, T)/G'_{rec}(\tau, T)$ in the pseudo-scalar and scalar channels in the deconfined phase. As once can see from the figure these ratios show no strong temperature dependence

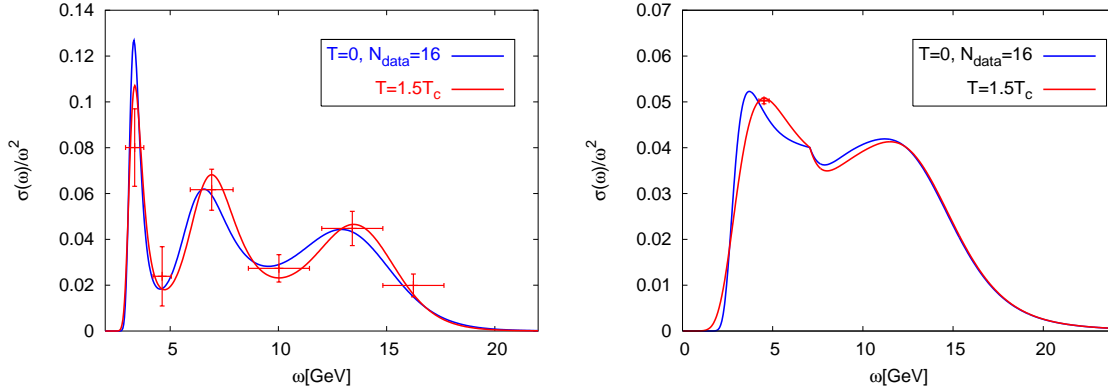


Figure 21. The spectral functions in pseudo-scalar channel calculated at $T = 1.5T_c$ and compared to the zero temperature spectral function obtained using $\tau_{max} = 1/(2T)$. In the left panel the spectral functions obtained with $m(\omega) = const$ are shown, while in the right panel the default model was obtained from the $T = 0$ spectral function.

and are close to one for all temperatures, including the highest temperature of $3T_c$. This means that the large temperature dependence seen in G/G_{rec} for the scalar and axial-vector channels comes mostly from the temperature dependence of $G_{low}(\tau, T)$ and is not related to melting of P-wave charmonium states. A question arises how the observed temperature (in)dependence of $G_{high}(\tau, T)$ is related to the expected in-medium modification of the heavy quark potential and melting of quarkonium states at sufficiently high temperatures. This question was addressed in Refs. [197], where the quarkonium spectral functions have been calculated using potential model with screened potential. It was found that despite the significant change in the spectral functions the Euclidean correlator obtained from them do not change significantly in the deconfined medium and are compatible with the lattice results. Including the imaginary part in the analysis did not change this conclusion [199]. Attempts to reconstruct quarkonium spectral functions using MEM have been presented in Refs. [186, 188, 189, 190, 201] and no evidence for melting of quarkonium states has been found. However, in view of the difficulties related to the MEM analysis for small τ_{max} and limited number of data points one should be careful drawing conclusions. In particular the dependence of the results on the default model should be examined. In Fig. 21 I show charmonium spectral functions in the pseudo-scalar channel calculated at $1.5T_c$ and at zero temperature for two default models: $m(\omega) = const$ and $m(\omega)$ that equals to the zero temperature spectral function for $\omega > 5$ GeV and smoothly matched to a constant below that energy [201]. In both cases the difference between the spectral function at $1.5T_c$ and $T = 0$ is small. However, the shape of the spectral function depends on the default model. While for $m(\omega) = const$ we see a peak structure for more realistic choice of the default model this peak structure is absent even at zero temperature. Recent analysis of charmonium spectral function based on isotropic lattices that uses free lattice spectral function also does not find peak structure that can be associated with 1S state in the deconfined phase [206] It is not clear to what extent the absence of bound state peaks is consequence of

quarkonium melting in QGP or due to the limited data set. It is clear, however, that existing MEM calculations of the spectral function do not provide evidence for existence of quarkonium bound states in QGP.

The analysis described so far was performed in the quenched approximation. Calculation of the charmonium correlators and spectral functions was also performed in two flavor QCD [207]. The findings of this analysis are similar to the ones described above. Furthermore, in the case of the bottomonium correlators and spectral functions have been studied using NRQCD [208, 209]. The main advantage of the NRQCD approach is that it allows to study correlators at larger Euclidean time separations, namely $\tau_{max} = 1/T$. Furthermore, there is no low energy contribution to the spectral functions and thus the temperature dependence of the corresponding Euclidean time correlation function is directly related to the properties and melting of the bound states. A significant temperature dependence has been seen in the scalar bottomonium correlators that may indicate the melting of the P-wave bottomonium at temperatures slightly above the transition temperature.

7.2. Meson spectral functions at non-zero temperature in the light quark sector

Early attempts to calculate light meson spectral functions in QGP using MEM were presented in Refs. [180, 183, 185, 187]. The results were inconclusive and to some extent confusing as peak structures in the spectral functions have been found up to $3T_c$ and no continuum was observed at high energies. It was pointed out, however, that even without using MEM Euclidean correlation functions can put stringent constraints on the spectral functions [180, 187]. In the vector channel the correlation function calculated on $N_\tau = 12$ and $N_\tau = 16$ lattices was found to deviate from the free value by less than 10% [180]. In the pseudo-scalar channel on the other hand a large enhancement over the free theory result was observed [187] possibly indicating non-perturbative effects in QGP.

More recently a detailed calculation of the vector correlation function on large quenched lattices was reported for $T \simeq 1.45T_c$ [210]. Calculations were performed using several lattice spacings. This enabled a reliable extrapolation to the continuum limit and it was found that the correlator never exceeds the free theory value by more than 9% [210]. The corresponding results are shown in Fig. 22. Furthermore, the spectral functions reconstructed with MEM showed no evidence for peak like structures [210]. Since vector correlator is so close to the free limit the authors of Ref. [210] obtained the spectral function using the following model

$$\begin{aligned}\sigma_{ii}(\omega) &= c_{BW} \chi_q \frac{1}{\pi} \frac{\omega \Gamma/2}{\omega^2 + (\Gamma/2)^2} + \frac{3}{2\pi} (1+k) \omega^2 \tanh(\omega/4T) \Theta(\omega_0, \Delta_\omega), \\ \Theta(\omega_0, \Delta_\omega) &= (1 + e^{(\omega_0 - \omega)/\omega \Delta_\omega})^{-1},\end{aligned}\tag{82}$$

and treating c_{BW} , Γ and k as fit parameters. Furthermore, several choices for the parameters ω_0 and Δ_ω have been considered, including $\omega_0 = \Delta_\omega = 0$. These fits are

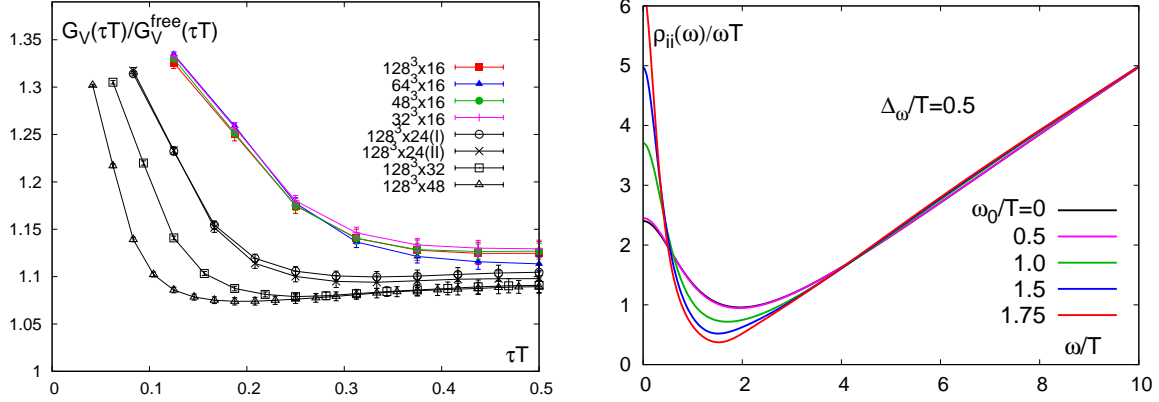


Figure 22. The vector correlation function, $G_V(\tau, T)$ calculated on different lattices for $T = 1.45T_c$ (left) and the vector spectral function (right) obtained using the fit form given by Eq. (82).

shown in Fig. 82 and gave the following constrains for the electric conductivity[210]

$$1/3 < \frac{1}{C_{em}} \frac{\zeta}{T} < 1, \quad C_{em} = \sum_f Q_f^2 \quad (83)$$

The disconnected part was neglected in this calculation. One can see from Fig. 22 that while somewhat broad the transport peak is clearly visible in the vector spectral function contrary to the expectation based in strongly coupled supersymmetric Yang-Mills theory where the transport peak is absent [211]. On the other hand the analysis of the same lattice data using a different approach lead to much smaller value of the electric conductivity and no clear transport peak [174]. This may indicate that much more work is needed till a reliable result for the electric conductivity can be quoted.

7.3. Spatial meson correlation functions

As discussed above spatial meson correlators are also sensitive to in-medium modification of the meson spectral functions. In particular, the change in the meson spectral functions is reflected in the meson screening masses, which should be close to the vacuum masses at low temperatures. At high temperatures, on the other hand, the meson screening masses should approach $2\pi T$ corresponding to the free quark limit. In the past meson screening masses have been studied in quenched approximation [212, 213] and the sharp change in their behavior was observed at the transition temperature. More recently spatial meson correlators and screening masses have been studied in 2+1 flavor QCD for physical strange quark mass and light quark masses $m_l = m_s/10$ with $p4$ action [141]. In the case of full QCD rapid change of the spatial correlators and screening masses is expected in the vicinity of the chiral crossover. Numerical calculations show that this is indeed the case [141]. In Fig. 23 the meson screening masses in the pseudo-scalar and vector channels are shown as function of the temperature and the rapid change in the behavior of the screening masses takes place around 200MeV, which is close to the

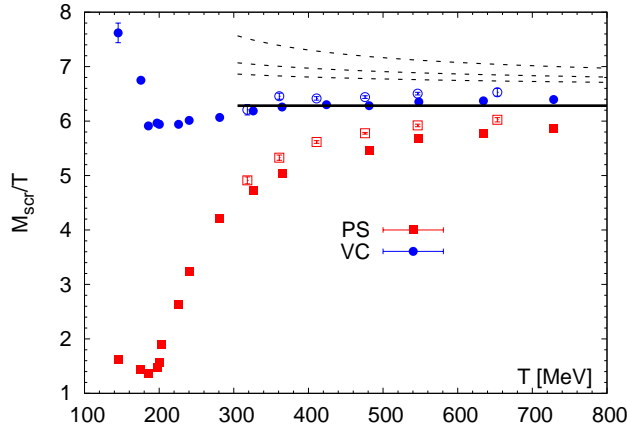


Figure 23. Meson screening masses for light quarks in the pseudo-scalar and vector channels as function of the temperature calculated in 2+1 flavor QCD with $p4$ action on $N_\tau = 6$ (filled symbols) and $N_\tau = 8$ (open symbols) lattices [141]. The solid black line corresponds to the limit of free quarks $2\pi T$. The dashed lines are the NLO results [214] evaluated with a 2-loop running coupling constant in \overline{MS} -scheme for $\mu = \pi T$, $2\pi T$ and $4\pi T$.

chiral crossover temperature T_c for those lattices. The effective restoration of the chiral symmetry above the crossover temperature should manifest in approximate degeneracy of the vector and axial-vector correlation functions. Such degeneracy is observed at temperature 200MeV (c.f. Fig. 5 of Ref. [141]). As discussed in section 5 the $U_A(1)$ symmetry is expected to be restored at sufficiently high temperatures. The effective restoration of the $U_A(1)$ should manifest itself in the approximate degeneracy of flavor non-singlet pseudo-scalar and scalar correlators. The difference between the scalar and pseudo-scalar screening masses rapidly decreases above the transition temperature but becomes compatible with zero only temperatures above 240MeV. Thus the effective restoration of the axial symmetry happens at $T \simeq 1.2T_c$, with T_c being the chiral transition temperature. Calculations using DWF formulations confirm this result [140].

At high temperatures the screening masses can be calculated using weak coupling methods. The calculations of the screening masses up to next-to-leading order was performed in Ref. [214] and the first perturbative correction turned out to be positive, namely

$$M_{scr} = 2\pi T + \frac{4}{3} \frac{T}{2\pi} g^2 \left(\frac{1}{2} + \hat{E}_0 \right), \quad (84)$$

with $\hat{E}_0 \simeq 0.46939139$ for $N_f = 3$ [214]. Furthermore, all the screening masses are expected to be degenerate at next-to-leading order [214]. In Fig. 23 we compare the lattice data in 2+1 flavor case with the perturbative result of Ref. [214]. At high temperatures we still see significant differences between the pseudo-scalar and vector screening masses. Moreover the pseudo-scalar screening masses are smaller than $2\pi T$. Note, however, that the lattice spacing (N_τ) dependence of the screening masses is

non-negligible. Thus it will be important in the future to perform calculations on finer lattices to get control over the continuum limit.

Spatial meson correlators and screening masses have been calculated also for charmonium [215]. The changes in the correlators and screening masses around the transition temperature are much smaller than for the light mesons. This fits into the picture that ground state charmonium does not melt at the crossover temperature. However, for $T > 300\text{MeV}$ we see large change also for the charmonium screening masses. The behavior of the screening masses and their dependence on the spatial boundary conditions is compatible with the picture of unbound quarks [215]. This corroborates the discussion in the previous subsection that there is no evidence for survival of charmonium states at temperatures of $1.5T_c$.

7.4. Heavy quark diffusion constant

Since for sufficiently heavy quarks the transport peak is very narrow it is very difficult if not impossible to determine the heavy quark diffusion using the procedure that was used for the electric conductivity $\dagger\dagger$. Even for the smallest possible heavy quark diffusion constant $D \simeq 1/(2\pi T)$ the low energy part of the vector correlator $G_{\text{low}}(\tau, T)$ shows very little τ -dependence [204]. An alternative way to estimate the heavy quark diffusion constant is integrate out the heavy quark fields and relate the drag coefficient to the correlation function of chromo-electric fields at time t and time 0 connected by Wilson lines [217, 218]. In particular, at leading order in the expansion in the inverse of heavy quark mass we have

$$\begin{aligned}\kappa &= \int dt G_E(t) \\ G_E(t) &= \frac{1}{3T\chi_q} \int d^3x \langle O_E^i(t, x) O_E^i(0, 0) \rangle \\ O_E^i(t, x) &= \phi^\dagger(t, x) g E^i(t, x) \phi(t, x) - \theta^\dagger(t, x) g E^i(t, x) \theta(t, x).\end{aligned}\tag{85}$$

Here ϕ and θ are the static quark and anti-quark fields, and E^i is the chromo-electric field. It is easy to generalize the above expression to Euclidean time and define the corresponding correlator $G_E(\tau)$ which after integrating the heavy quark fields becomes [218]

$$G_E(\tau) = -\frac{1}{3} \frac{\langle \text{ReTr} (W(\beta, \tau) g E_i(\tau) W(\tau, 0) E_i(\tau)) \rangle}{\text{ReTr} \langle W(\beta, 0) \rangle}.\tag{86}$$

The above correlation function was also calculated in perturbation theory to next-to-leading order [218]. The key difference between this correlation function and meson correlation function is that the transport contribution does not appear as a narrow peak in the corresponding spectral function. This in principle should make it easier to estimate the corresponding transport coefficient. Numerical calculations of $G_E(\tau)$ have been performed in $SU(3)$ gauge theory on lattices with temporal extent $N_\tau = 12 - 24$ [219, 220, 221]. The lattice data are significantly larger than the next-to-leading order

$\dagger\dagger$ attempts along these lines have been presented in Ref. [216]

result. Comparing the numerical results with a model correlation function based on perturbative calculations of Ref. [218] and strong coupling calculations in $N = 4$ Super-Yang-Mills theory [217] it was concluded that the heavy quark diffusion constant should be in the range

$$D = (0.5 - 1.0)/T. \quad (87)$$

The above value is considerably smaller than the perturbative estimate [175] and lies in the range used in phenomenological models [168].

8. Conclusions

In recent years significant progress has been made in studying chiral and deconfining aspects of the QCD transition in finite temperature QCD. For several quantities that are relevant for the discussion of these aspects continuum extrapolation has been performed. Calculations by two groups that use different staggered quark formulation give results for the chiral transition temperature that agree in the continuum limit. It is now established that for physical value of chiral transition temperature is $T_c \simeq 150\text{MeV}$. Calculations using Wilson fermion or DWF formulation have been performed for physical or nearly physical quark masses and seem to confirm the staggered fermion results. The universal behavior of the chiral transition in the limit of vanishing light quark masses plays an important role also for the physical values of the light quark masses and allows to define the chiral crossover temperature in a meaningful way.

The interplay between chiral and deconfinement aspects of the transition appears to be more complicated than earlier lattice studies suggested. There is no transition temperature that can be associated with the deconfining aspects of the transition for physical values of the light quark masses. Furthermore, the behavior of the Polyakov loop suggests that color screening sets in at temperatures that are higher than the chiral transition temperature. The deconfinement aspects of the QCD transition have been also studied in terms of fluctuations of conserved charges. In principle these fluctuations are also sensitive to universal aspects of the chiral transition. However, for the lowest order, i.e. quadratic fluctuations the contribution coming from the regular part of the free energy density dominates. This implies in particular, that inflection points of the quark number susceptibilities cannot be used to define the transition temperature. Higher order fluctuations of conserved charges are more sensitive to the singular contribution and therefore are more suitable to study the interplay between chiral and deconfining aspects of the QCD transition at finite temperature. The restoration of the $U_A(1)$ symmetry at high temperature has been also discussed and it was found that it is effectively restored at temperatures $T \simeq 1.2T_c$.

In the high temperature region ($T > 300\text{ MeV}$) lattice results have been compared with the results obtained in weak coupling approaches, which seem to capture the qualitative features of the lattice data. In some cases we see a good agreement at quantitative level.

Finally I discussed lattice results on meson correlation functions. These are useful to study the fate of quarkonium states in QGP as well as for determination of some transport coefficients. While a lot of progress has been made in studying meson correlation functions and extracting the corresponding spectral functions more work is needed to reach definitive conclusions.

Acknowledgments

This work was supported by U.S. Department of Energy under Contract No. DE-AC02-98CH10886. I would like to thank Rob Pisarski and Swagato Mukherjee for useful discussions.

- [1] R. Hagedorn, *Nuovo Cim. Suppl.* **3**, 147 (1965).
- [2] N. Cabibbo and G. Parisi, *Phys. Lett.* **B59**, 67 (1975).
- [3] J. C. Collins and M. Perry, *Phys.Rev.Lett.* **34**, 1353 (1975).
- [4] E. V. Shuryak, *Phys.Rept.* **61**, 71 (1980).
- [5] E. V. Shuryak, *Sov. Phys. JETP* **47**, 212 (1978).
- [6] A. M. Polyakov, *Phys.Lett.* **B72**, 477 (1978).
- [7] L. Susskind, *Phys.Rev.* **D20**, 2610 (1979).
- [8] J. Kuti, J. Polonyi, and K. Szlachanyi, *Phys. Lett.* **B98**, 199 (1981).
- [9] L. D. McLerran and B. Svetitsky, *Phys. Rev.* **D24**, 450 (1981).
- [10] J. Engels, F. Karsch, H. Satz, and I. Montvay, *Phys. Lett.* **B101**, 89 (1981).
- [11] A. D. Linde, *Phys.Lett.* **B96**, 289 (1980).
- [12] M. Hindmarsh and O. Philipsen, *Phys.Rev.* **D71**, 087302 (2005), hep-ph/0501232.
- [13] T. Asaka, M. Laine, and M. Shaposhnikov, *JHEP* **0606**, 053 (2006), hep-ph/0605209.
- [14] M. Laine, *PoS LAT2006*, 014 (2006), hep-lat/0612023.
- [15] B. Muller and J. L. Nagle, *Ann.Rev.Nucl.Part.Sci.* **56**, 93 (2006), nucl-th/0602029.
- [16] T. Muta, *World Sci.Lect.Notes Phys.* **57**, 1 (1998).
- [17] D. J. Gross, R. D. Pisarski, and L. G. Yaffe, *Rev.Mod.Phys.* **53**, 43 (1981).
- [18] R. D. Pisarski and F. Wilczek, *Phys. Rev.* **D29**, 338 (1984).
- [19] C. Alexandrou *et al.*, *Phys.Rev.* **D60**, 034504 (1999), hep-lat/9811028.
- [20] F. Karsch, C. Schmidt, and S. Sticka, *Comput.Phys.Commun.* **147**, 451 (2002), hep-lat/0111059.
- [21] WHOT-QCD Collaboration, H. Saito *et al.*, *Phys.Rev.* **D84**, 054502 (2011), 1106.0974.
- [22] T. Herpay, A. Patkos, Z. Szepe, and P. Szepfalussy, *Phys.Rev.* **D71**, 125017 (2005), hep-ph/0504167.
- [23] T. Herpay and Z. Szepe, *Phys.Rev.* **D74**, 025008 (2006), hep-ph/0604086.
- [24] F. Karsch *et al.*, *Nucl.Phys.Proc.Suppl.* **129**, 614 (2004), hep-lat/0309116.
- [25] G. Endrodi, Z. Fodor, S. Katz, and K. Szabo, *PoS LAT2007*, 182 (2007), 0710.0998.
- [26] H.-T. Ding *et al.*, (2011), 1111.0185.
- [27] Y. Aoki, G. Endrodi, Z. Fodor, S. Katz, and K. Szabo, *Nature* **443**, 675 (2006), hep-lat/0611014.
- [28] MILC Collaboration, C. Bernard *et al.*, *Phys. Rev.* **D71**, 034504 (2005), hep-lat/0405029.
- [29] M. Cheng *et al.*, *Phys. Rev.* **D74**, 054507 (2006), hep-lat/0608013.
- [30] K. G. Wilson, *Phys. Rev.* **D10**, 2445 (1974).
- [31] M. Luscher and P. Weisz, *Commun.Math.Phys.* **97**, 59 (1985).
- [32] T. DeGrand and C. E. Detar, *Lattice methods for quantum chromodynamics* (World Scientific, 2006).
- [33] D. B. Kaplan, *Phys.Lett.* **B288**, 342 (1992), hep-lat/9206013.
- [34] V. Furman and Y. Shamir, *Nucl.Phys.* **B439**, 54 (1995), hep-lat/9405004.
- [35] Y. Shamir, *Nucl.Phys.* **B406**, 90 (1993), hep-lat/9303005.

- [36] Y. Shamir, Phys.Rev. **D71**, 034509 (2005), hep-lat/0412014.
- [37] Y. Shamir, Phys.Rev. **D75**, 054503 (2007), hep-lat/0607007.
- [38] S. R. Sharpe, PoS **LAT2006**, 022 (2006), hep-lat/0610094.
- [39] D. H. Adams, Phys.Rev. **D77**, 105024 (2008), 0802.3029.
- [40] C. Bernard, M. Golterman, Y. Shamir, and S. R. Sharpe, Phys.Lett. **B649**, 235 (2007), hep-lat/0603027.
- [41] C. Bernard, M. Golterman, and Y. Shamir, Phys.Rev. **D77**, 074505 (2008), 0712.2560.
- [42] C. Bernard, M. Golterman, Y. Shamir, and S. R. Sharpe, Phys.Rev. **D77**, 114504 (2008), 0711.0696.
- [43] M. Creutz, PoS **CONFINEMENT8**, 016 (2008), 0810.4526.
- [44] U. M. Heller, F. Karsch, and B. Sturmfels, Phys. Rev. **D60**, 114502 (1999), hep-lat/9901010.
- [45] APE, M. Albanese *et al.*, Phys. Lett. **B192**, 163 (1987).
- [46] MILC Collaboration, K. Orginos, D. Toussaint, and R. Sugar, Phys. Rev. **D60**, 054503 (1999), hep-lat/9903032.
- [47] A. Hasenfratz and F. Knechtli, Phys. Rev. **D64**, 034504 (2001), hep-lat/0103029.
- [48] A. Hasenfratz, Nucl. Phys. Proc. Suppl. **119**, 131 (2003), hep-lat/0211007.
- [49] A. Hasenfratz, R. Hoffmann, and S. Schaefer, JHEP **0705**, 029 (2007), hep-lat/0702028.
- [50] HPQCD Collaboration, UKQCD Collaboration, E. Follana *et al.*, Phys. Rev. **D75**, 054502 (2007), hep-lat/0610092.
- [51] Y. Aoki, Z. Fodor, S. Katz, and K. Szabo, JHEP **0601**, 089 (2006), hep-lat/0510084.
- [52] Y. Aoki, Z. Fodor, S. Katz, and K. Szabo, Phys. Lett. **B643**, 46 (2006), hep-lat/0609068.
- [53] Y. Aoki *et al.*, JHEP **0906**, 088 (2009), 0903.4155.
- [54] M. Clark, P. de Forcrand, and A. Kennedy, PoS **LAT2005**, 115 (2006), hep-lat/0510004.
- [55] MILC Collaboration, A. Bazavov *et al.*, PoS **LATTICE2010**, 074 (2010), 1012.0868.
- [56] A. Bazavov *et al.*, Phys. Rev. **D85**, 054503 (2012), 1111.1710.
- [57] M. Le Bellac, *Thermal field theory* Cambridge monographs on mathematical physics (Cambridge Univ. Press, Cambridge, 1996).
- [58] K. Holland, M. Pepe, and U. Wiese, Nucl.Phys.Proc.Suppl. **129**, 712 (2004), hep-lat/0309062.
- [59] K. Holland, M. Pepe, and U. Wiese, Nucl.Phys. **B694**, 35 (2004), hep-lat/0312022.
- [60] M. Pepe and U.-J. Wiese, Nucl.Phys. **B768**, 21 (2007), hep-lat/0610076, Dedicated to Peter Minkowski on the occasion of his 65th birthday.
- [61] O. Kaczmarek, F. Karsch, E. Laermann, and M. Lutgemeier, Phys. Rev. **D62**, 034021 (2000), hep-lat/9908010.
- [62] S. Digal, S. Fortunato, and P. Petreczky, Phys. Rev. **D68**, 034008 (2003), hep-lat/0304017.
- [63] Y. Burnier, M. Laine, and M. Vepsäläinen, JHEP **1001**, 054 (2010), 0911.3480.
- [64] N. Brambilla, J. Ghiglieri, P. Petreczky, and A. Vairo, Phys.Rev. **D82**, 074019 (2010), 1007.5172.
- [65] S. Nadkarni, Phys. Rev. **D33**, 3738 (1986).
- [66] S. Nadkarni, Phys. Rev. **D34**, 3904 (1986).
- [67] O. Jahn and O. Philipsen, Phys. Rev. **D70**, 074504 (2004), hep-lat/0407042.
- [68] M. Doring, K. Huebner, O. Kaczmarek, and F. Karsch, Phys.Rev. **D75**, 054504 (2007), hep-lat/0702009.
- [69] S. Gupta, K. Huebner, and O. Kaczmarek, Phys.Rev. **D77**, 034503 (2008), 0711.2251.
- [70] A. Mykkanen, M. Panero, and K. Rummukainen, (2012), 1202.2762.
- [71] P. Petreczky, Eur. Phys. J. **C43**, 51 (2005), hep-lat/0502008.
- [72] N. Brambilla, A. Pineda, J. Soto, and A. Vairo, Nucl. Phys. **B566**, 275 (2000), hep-ph/9907240.
- [73] N. Brambilla, J. Ghiglieri, A. Vairo, and P. Petreczky, Phys. Rev. **D78**, 014017 (2008), 0804.0993.
- [74] Wuppertal-Budapest Collaboration, S. Borsanyi *et al.*, JHEP **1009**, 073 (2010), 1005.3508.
- [75] O. Kaczmarek, F. Karsch, P. Petreczky, and F. Zantow, Phys. Lett. **B543**, 41 (2002), hep-lat/0207002.
- [76] O. Kaczmarek and F. Zantow, Phys. Rev. **D71**, 114510 (2005), hep-lat/0503017.
- [77] P. Petreczky and K. Petrov, Phys. Rev. **D70**, 054503 (2004), hep-lat/0405009.

- [78] P. Petreczky, J.Phys.G **G37**, 094009 (2010), 1001.5284.
- [79] O. Kaczmarek, PoS **CPOD07**, 043 (2007), 0710.0498.
- [80] Y. Maezawa *et al.*, (2011), 1112.2756.
- [81] Z. Fodor, A. Jakovac, S. Katz, and K. Szabo, PoS **LAT2007**, 196 (2007), 0710.4119.
- [82] P. Petreczky *et al.*, Nucl. Phys. **A698**, 400 (2002), hep-lat/0103034.
- [83] O. Kaczmarek, F. Karsch, F. Zantow, and P. Petreczky, Phys.Rev. **D70**, 074505 (2004), hep-lat/0406036.
- [84] A. K. Rebhan, Phys. Rev. **D48**, 3967 (1993), hep-ph/9308232.
- [85] A. K. Rebhan, Nucl. Phys. **B430**, 319 (1994), hep-ph/9408262.
- [86] A. Patkos, P. Petreczky, and Z. Szep, Eur.Phys.J. **C5**, 337 (1998), hep-ph/9711263.
- [87] M. Cheng *et al.*, Phys. Rev. **D77**, 014511 (2008), 0710.0354.
- [88] A. Bazavov, P. Petreczky, and A. Velytsky, Phys. Rev. **D78**, 114026 (2008), 0809.2062.
- [89] U. M. Heller, F. Karsch, and J. Rank, Phys.Lett. **B355**, 511 (1995), hep-lat/9505016.
- [90] U. M. Heller, F. Karsch, and J. Rank, Phys.Rev. **D57**, 1438 (1998), hep-lat/9710033.
- [91] F. Karsch, M. Oevers, and P. Petreczky, Phys.Lett. **B442**, 291 (1998), hep-lat/9807035.
- [92] A. Cucchieri, F. Karsch, and P. Petreczky, Phys.Rev. **D64**, 036001 (2001), hep-lat/0103009.
- [93] A. Nakamura, T. Saito, and S. Sakai, Phys.Rev. **D69**, 014506 (2004), hep-lat/0311024.
- [94] A. Cucchieri and T. Mendes, (2012), 1201.6086.
- [95] A. Cucchieri, F. Karsch, and P. Petreczky, Phys.Lett. **B497**, 80 (2001), hep-lat/0004027.
- [96] D. Karabali, C.-j. Kim, and V. Nair, Nucl.Phys. **B524**, 661 (1998), hep-th/9705087.
- [97] V. Nair, (1998), hep-th/9809086.
- [98] V. Nair, Nucl.Phys.Proc.Suppl. **108**, 194 (2002), hep-th/0204063.
- [99] G. D. Moore, p. 82 (2000), hep-ph/0009161.
- [100] T. Appelquist and R. D. Pisarski, Phys.Rev. **D23**, 2305 (1981).
- [101] E. Braaten and A. Nieto, Phys.Rev. **D53**, 3421 (1996), hep-ph/9510408.
- [102] K. Kajantie, M. Laine, K. Rummukainen, and M. E. Shaposhnikov, Nucl.Phys. **B503**, 357 (1997), hep-ph/9704416.
- [103] A. Hart and O. Philipsen, Nucl.Phys. **B572**, 243 (2000), hep-lat/9908041.
- [104] A. Hart, M. Laine, and O. Philipsen, Nucl.Phys. **B586**, 443 (2000), hep-ph/0004060.
- [105] M. Laine and Y. Schroder, JHEP **0503**, 067 (2005), hep-ph/0503061.
- [106] S.-J. Sin and I. Zahed, Phys.Lett. **B648**, 318 (2007), hep-ph/0606049.
- [107] O. Andreev and V. I. Zakharov, Phys.Lett. **B645**, 437 (2007), hep-ph/0607026.
- [108] O. Andreev, Phys.Lett. **B659**, 416 (2008), 0709.4395.
- [109] J. Alanen, K. Kajantie, and V. Suur-Uski, Phys.Rev. **D80**, 075017 (2009), 0905.2032.
- [110] K. Kajantie *et al.*, Phys.Rev.Lett. **79**, 3130 (1997), hep-ph/9708207.
- [111] M. Laine and O. Philipsen, Nucl.Phys. **B523**, 267 (1998), hep-lat/9711022.
- [112] M. Laine and O. Philipsen, Phys.Lett. **B459**, 259 (1999), hep-lat/9905004.
- [113] S. Datta and S. Gupta, Nucl.Phys. **B534**, 392 (1998), hep-lat/9806034.
- [114] S. Datta and S. Gupta, Phys.Lett. **B471**, 382 (2000), hep-lat/9906023.
- [115] S. Datta and S. Gupta, Phys.Rev. **D67**, 054503 (2003), hep-lat/0208001.
- [116] P. B. Arnold and L. G. Yaffe, Phys.Rev. **D52**, 7208 (1995), hep-ph/9508280.
- [117] E. Braaten and A. Nieto, Phys.Rev.Lett. **74**, 3530 (1995), hep-ph/9410218.
- [118] M. Laine and M. Vepsalainen, JHEP **0909**, 023 (2009), 0906.4450.
- [119] R. Fiore, A. Papa, and P. Provero, Phys.Rev. **D67**, 114508 (2003), hep-lat/0302004.
- [120] HotQCD collaboration, A. Bazavov and P. Petreczky, J.Phys.Conf.Ser. **230**, 012014 (2010), 1005.1131.
- [121] M. Cheng *et al.*, Phys.Rev. **D79**, 074505 (2009), 0811.1006.
- [122] A. Bazavov *et al.*, Phys. Rev. **D80**, 014504 (2009), 0903.4379.
- [123] RBC-Bielefeld Collaboration, P. Petreczky, P. Hegde, and A. Velytsky, PoS **LAT2009**, 159 (2009), 0911.0196.
- [124] S. Mukherjee, J.Phys.G **G38**, 124022 (2011), 1107.0765.

- [125] P. Hegde and f. t. H. Collaboration, (2011), 1110.5932.
- [126] for HotQCD collaboration, A. Bazavov, (2012), 1201.5345.
- [127] S. Borsanyi *et al.*, JHEP **1201**, 138 (2012), 1112.4416.
- [128] HotQCD Collaboration, A. Bazavov *et al.*, (2012), 1203.0784.
- [129] S. Borsanyi *et al.*, (2011), 1111.3500.
- [130] J. Blaizot, E. Iancu, and A. Rebhan, Phys.Lett. **B523**, 143 (2001), hep-ph/0110369.
- [131] A. Rebhan, (2003), hep-ph/0301130.
- [132] N. Haque and M. G. Mustafa, (2010), 1007.2076.
- [133] A. Hietanen and K. Rummukainen, JHEP **0804**, 078 (2008), 0802.3979.
- [134] V. Koch, A. Majumder, and J. Randrup, Phys.Rev.Lett. **95**, 182301 (2005), nucl-th/0505052.
- [135] P. Huovinen and P. Petreczky, Nucl. Phys. **A837**, 26 (2010), 0912.2541.
- [136] P. Huovinen and P. Petreczky, J.Phys.Conf.Ser. **230**, 012012 (2010), 1005.0324.
- [137] P. Huovinen and P. Petreczky, J.Phys.G **G38**, 124103 (2011), 1106.6227.
- [138] P. Petreczky, Nucl.Phys. **A830**, 11C (2009), 0908.1917.
- [139] S. Ejiri *et al.*, Phys. Rev. **D80**, 094505 (2009), 0909.5122.
- [140] P. Hegde, (2011), 1112.0364.
- [141] M. Cheng *et al.*, Eur.Phys.J. **C71**, 1564 (2011), 1010.1216.
- [142] O. Kaczmarek *et al.*, Phys. Rev. **D83**, 014504 (2011), 1011.3130.
- [143] J. Engels, S. Holtmann, T. Mendes, and T. Schulze, Phys. Lett. **B492**, 219 (2000), hep-lat/0006023.
- [144] D. Toussaint, Phys. Rev. **D55**, 362 (1997), hep-lat/9607084.
- [145] J. Engels and T. Mendes, Nucl. Phys. **B572**, 289 (2000), hep-lat/9911028.
- [146] J. Engels, S. Holtmann, T. Mendes, and T. Schulze, Phys. Lett. **B514**, 299 (2001), hep-lat/0105028.
- [147] J. Engels and F. Karsch, (2011), 1105.0584.
- [148] Z. Fodor and S. Katz, JHEP **0203**, 014 (2002), hep-lat/0106002.
- [149] Z. Fodor and S. Katz, JHEP **0404**, 050 (2004), hep-lat/0402006.
- [150] P. de Forcrand and O. Philipsen, Nucl.Phys. **B642**, 290 (2002), hep-lat/0205016.
- [151] P. de Forcrand and O. Philipsen, JHEP **0701**, 077 (2007), hep-lat/0607017.
- [152] R. Falcione, E. Laermann, and M. P. Lombardo, PoS **LATTICE2010**, 183 (2010), 1012.4694, 7 pages, 12 figures, talk presented at the XXVIII International Symposium on Lattice Field Theory (Lattice 2010), June 14-19, 2010, Villasimius, Sardinia, Italy.
- [153] S. Borsanyi *et al.*, JHEP **1011**, 077 (2010), 1007.2580.
- [154] M. Cheng *et al.*, Phys. Rev. **D81**, 054504 (2010), 0911.2215.
- [155] for the HotQCD Collaboration, A. Bazavov and P. Petreczky, PoS **LATTICE2010**, 169 (2010), 1012.1257.
- [156] HotQCD collaboration, W. Soldner, PoS **LATTICE2010**, 215 (2010), 1012.4484.
- [157] F. Karsch, E. Laermann, and A. Peikert, Phys.Lett. **B478**, 447 (2000), hep-lat/0002003.
- [158] F. Csikor *et al.*, JHEP **0405**, 046 (2004), hep-lat/0401016.
- [159] J. Blaizot, E. Iancu, and A. Rebhan, Phys.Rev.Lett. **83**, 2906 (1999), hep-ph/9906340.
- [160] J. Blaizot, E. Iancu, and A. Rebhan, Phys.Rev. **D63**, 065003 (2001), hep-ph/0005003.
- [161] S. S. Gubser, I. R. Klebanov, and A. A. Tseytlin, Nucl.Phys. **B534**, 202 (1998), hep-th/9805156.
- [162] J. O. Andersen, L. E. Leganger, M. Strickland, and N. Su, Phys.Lett. **B696**, 468 (2011), 1009.4644.
- [163] R. Rapp *et al.*, Lect.Notes Phys. **814**, 335 (2011).
- [164] T. Matsui and H. Satz, Phys. Lett. **B178**, 416 (1986).
- [165] Quarkonium Working Group, N. Brambilla *et al.*, (2004), hep-ph/0412158.
- [166] N. Brambilla *et al.*, Eur.Phys.J. **C71**, 1534 (2011), 1010.5827.
- [167] A. Bazavov, P. Petreczky, and A. Velytsky, (2009), 0904.1748.
- [168] R. Rapp and H. van Hees, (2009), 0903.1096.
- [169] L. D. McLerran and T. Toimela, Phys.Rev. **D31**, 545 (1985).

- [170] E. Braaten, R. D. Pisarski, and T.-C. Yuan, *Phys. Rev. Lett.* **64**, 2242 (1990).
- [171] F. Karsch, E. Laermann, P. Petreczky, and S. Sticka, *Phys. Rev.* **D68**, 014504 (2003), hep-lat/0303017.
- [172] G. Aarts and J. M. Martinez Resco, *Nucl. Phys.* **B726**, 93 (2005), hep-lat/0507004.
- [173] H. B. Meyer, *Eur.Phys.J.* **A47**, 86 (2011), 1104.3708.
- [174] Y. Burnier and M. Laine, (2012), 1201.1994.
- [175] G. D. Moore and D. Teaney, *Phys.Rev.* **C71**, 064904 (2005), hep-ph/0412346.
- [176] M. Asakawa, T. Hatsuda, and Y. Nakahara, *Prog. Part. Nucl. Phys.* **46**, 459 (2001), hep-lat/0011040.
- [177] G. P. Lepage *et al.*, *Nucl. Phys. Proc. Suppl.* **106**, 12 (2002), hep-lat/0110175.
- [178] R. K. Bryan, *Eur. Biophys. J.* **18**, 165 (1990).
- [179] Y. Nakahara, M. Asakawa, and T. Hatsuda, *Phys. Rev.* **D60**, 091503 (1999), hep-lat/9905034.
- [180] F. Karsch, E. Laermann, P. Petreczky, S. Sticka, and I. Wetzorke, *Phys. Lett.* **B530**, 147 (2002), hep-lat/0110208.
- [181] CP-PACS, T. Yamazaki *et al.*, *Phys. Rev.* **D65**, 014501 (2002), hep-lat/0105030.
- [182] I. Wetzorke, F. Karsch, E. Laermann, P. Petreczky, and S. Sticka, *Nucl.Phys.Proc.Suppl.* **106**, 510 (2002), hep-lat/0110132.
- [183] F. Karsch *et al.*, *Nucl. Phys.* **A715**, 701 (2003), hep-ph/0209028.
- [184] S. Datta, F. Karsch, P. Petreczky, and I. Wetzorke, *Nucl. Phys. Proc. Suppl.* **119**, 487 (2003), hep-lat/0208012.
- [185] M. Asakawa, T. Hatsuda, and Y. Nakahara, *Nucl. Phys.* **A715**, 863 (2003), hep-lat/0208059.
- [186] T. Umeda, K. Nomura, and H. Matsufuru, *Eur. Phys. J.* **C39S1**, 9 (2005), hep-lat/0211003.
- [187] P. Petreczky, *J. Phys.* **G30**, S431 (2004), hep-ph/0305189.
- [188] M. Asakawa and T. Hatsuda, *Phys. Rev. Lett.* **92**, 012001 (2004), hep-lat/0308034.
- [189] S. Datta, F. Karsch, P. Petreczky, and I. Wetzorke, *Phys. Rev.* **D69**, 094507 (2004), hep-lat/0312037.
- [190] S. Datta, F. Karsch, P. Petreczky, and I. Wetzorke, *J.Phys.G* **G30**, S1347 (2004), hep-lat/0403017.
- [191] T. Blum and P. Petreczky, *Nucl. Phys. Proc. Suppl.* **140**, 553 (2005), hep-lat/0408045.
- [192] K. Sasaki, S. Sasaki, and T. Hatsuda, *Phys. Lett.* **B623**, 208 (2005), hep-lat/0504020.
- [193] S. Datta, A. Jakovac, F. Karsch, and P. Petreczky, *AIP Conf. Proc.* **842**, 35 (2006), hep-lat/0603002.
- [194] M. Laine, O. Philipsen, P. Romatschke, and M. Tassler, *JHEP* **0703**, 054 (2007), hep-ph/0611300.
- [195] A. Mocsy and P. Petreczky, *Phys. Rev.* **D73**, 074007 (2006), hep-ph/0512156.
- [196] A. Mocsy and P. Petreczky, *Phys. Rev. Lett.* **99**, 211602 (2007), 0706.2183.
- [197] A. Mocsy and P. Petreczky, *Phys. Rev.* **D77**, 014501 (2008), 0705.2559.
- [198] A. Mocsy and P. Petreczky, *Eur. Phys. J. ST* **155**, 101 (2008), 0710.5125.
- [199] P. Petreczky, C. Miao, and A. Mocsy, *Nucl.Phys.* **A855**, 125 (2011), 1012.4433.
- [200] F. Riek and R. Rapp, *New J.Phys.* **13**, 045007 (2011), 1012.0019.
- [201] A. Jakovac, P. Petreczky, K. Petrov, and A. Velytsky, *Phys. Rev.* **D75**, 014506 (2007), hep-lat/0611017.
- [202] A. X. El-Khadra, A. S. Kronfeld, and P. B. Mackenzie, *Phys.Rev.* **D55**, 3933 (1997), hep-lat/9604004.
- [203] S. Datta, F. Karsch, S. Wissel, P. Petreczky, and I. Wetzorke, (2004), hep-lat/0409147.
- [204] P. Petreczky and D. Teaney, *Phys. Rev.* **D73**, 014508 (2006), hep-ph/0507318.
- [205] P. Petreczky, *Eur.Phys.J.* **C62**, 85 (2009), 0810.0258.
- [206] H.-T. Ding *et al.*, *PoS LATTICE2010*, 180 (2010), 1011.0695.
- [207] G. Aarts, C. Allton, M. B. Oktay, M. Peardon, and J.-I. Skullerud, *Phys. Rev.* **D76**, 094513 (2007), 0705.2198.
- [208] G. Aarts *et al.*, *Phys.Rev.Lett.* **106**, 061602 (2011), 1010.3725.
- [209] G. Aarts *et al.*, *JHEP* **1111**, 103 (2011), 1109.4496.

- [210] H.-T. Ding *et al.*, Phys.Rev. **D83**, 034504 (2011), 1012.4963.
- [211] D. Teaney, Phys.Rev. **D74**, 045025 (2006), hep-ph/0602044.
- [212] E. Laermann and P. Schmidt, Eur.Phys.J. **C20**, 541 (2001), hep-lat/0103037.
- [213] R. V. Gavai and S. Gupta, Phys.Rev. **D67**, 034501 (2003), hep-lat/0211015.
- [214] M. Laine and M. Vepsalainen, JHEP **0402**, 004 (2004), hep-ph/0311268.
- [215] F. Karsch, E. Laermann, S. Mukherjee, and P. Petreczky, (2012), 1203.3770.
- [216] H. Ding *et al.*, J.Phys.G **G38**, 124070 (2011), 1107.0311.
- [217] J. Casalderrey-Solana and D. Teaney, Phys.Rev. **D74**, 085012 (2006), hep-ph/0605199.
- [218] S. Caron-Huot, M. Laine, and G. D. Moore, JHEP **0904**, 053 (2009), 0901.1195.
- [219] H. B. Meyer, New J.Phys. **13**, 035008 (2011), 1012.0234.
- [220] D. Banerjee, S. Datta, R. Gavai, and P. Majumdar, (2011), 1109.5738.
- [221] A. Francis, O. Kaczmarek, M. Laine, and J. Langelage, (2011), 1109.3941.